

Climate Forcing and Salinity Variability in Chesapeake Bay, USA

Jiangtao Xu · Wen Long · Jerry D. Wiggert ·
Lyon W. J. Lanerolle · Christopher W. Brown ·
Raghu Murtugudde · Raleigh R. Hood

Received: 3 January 2011 / Revised: 3 June 2011 / Accepted: 17 June 2011 / Published online: 13 July 2011
© Coastal and Estuarine Research Federation 2011

Abstract Salinity is a critical factor in understanding and predicting physical and biogeochemical processes in the coastal ocean where it varies considerably in time and space. In this paper, we introduce a Chesapeake Bay community implementation of the Regional Ocean Modeling System (ChesROMS) and use it to investigate the interannual variability of salinity in Chesapeake Bay. The ChesROMS implementation was evaluated by quantitatively comparing the model solutions with the observed variations in the Bay for a 15-year period (1991 to 2005). Temperature fields were most consistently well predicted, with a correlation of 0.99 and a root mean square error (RMSE) of 1.5°C for the period, with modeled salinity following closely with a correlation of 0.94 and RMSE of 2.5. Variability of salinity anomalies from climatology based on modeled salinity was examined using empirical orthogonal function analysis, which indicates the

salinity distribution in the Bay is principally driven by river forcing. Wind forcing and tidal mixing were also important factors in determining the salinity stratification in the water column, especially during low flow conditions. The fairly strong correlation between river discharge anomaly in this region and the Pacific Decadal Oscillation suggests that the long-term salinity variability in the Bay is affected by large-scale climate patterns. The detailed analyses of the role and importance of different forcing, including river runoff, atmospheric fluxes, and open ocean boundary conditions, are discussed in the context of the observed and modeled interannual variability.

Keywords Chesapeake Bay · Skill assessment · Salinity variability · EOF analysis · Model validation · Estuary · Climate · Spatiotemporal patterns

J. Xu (✉) · L. W. J. Lanerolle
NOAA/NOS/OCS/CSDL,
1315 East-West Highway,
Silver Spring, MD 20910, USA
e-mail: Jiangtao.Xu@noaa.gov

J. Xu
UCAR,
P. O. Box 3000, FL-4/VSP/Suite 2200,
Boulder, CO 80307-3000, USA

W. Long · R. R. Hood
Horn Point Laboratory,
University of Maryland Center for Environmental Science,
2020 Horn Point Road,
Cambridge, MD 21613, USA

J. D. Wiggert
Department of Marine Sciences,
University of Southern Mississippi,
1020 Balch Boulevard,
Stennis Space Center, MS 39529, USA

L. W. J. Lanerolle
Earth Resources Technology (ERT) Inc.,
6100 Frost Place, Suite A,
Laurel, MD 20707, USA

C. W. Brown
NOAA, Center for Satellite Applications and Research,
5825 University Research Court, Suite 4001,
College Park, MD 20740, USA

R. Murtugudde
ESSIC/DAOS, University of Maryland,
CSS Bldg, Room 2201,
College Park, MD 20742, USA

Introduction

Chesapeake Bay has been used as a prototype for semi-enclosed, partially mixed estuarine system research for many years. Research focusing on its physical characteristics, such as tides (Hicks 1964), sea level fluctuations (Wang 1979a; Wang and Elliott 1978), and circulation (Elliott et al. 1978; Pritchard 1952; Schubel and Pritchard 1986), has led to major advances in our understanding of estuarine dynamics. For a partially mixed, microtidal estuary like Chesapeake Bay, with relatively large freshwater input, the longitudinal circulation is mainly density-driven and reveals a prototypical two-layer structure, which consists of a surface layer of fresher water flowing seaward and a saline return flow at depth.

The strength of the two-layer circulation in Chesapeake Bay is largely regulated by both the freshwater discharge rate and the atmospheric conditions (Elliott et al. 1978; Schubel and Pritchard 1986; Wang 1979b). The freshwater discharge into the Bay principally consists of the Susquehanna River at the head of the Bay (~48%) and the mid-Bay Potomac River inflow (~16%). Other, less concentrated freshwater inputs consist of the York, Rappahannock, and James Rivers (sum of ~19%) to the west and the rivers and streams along the Eastern Shore (adding up to ~10%) (Schubel and Pritchard 1986). The magnitude of river runoff peaks in the spring and is minimal in the later part of the summer, which strongly contributes to the regulation of the intensity of the longitudinal circulation that generally manifests from the Bay Bridge (39° N) to near the mouth of the Rappahannock River (37.6° N) (Xu et al. 2002). Elliott et al. (1978) examined the circulation near the head of Chesapeake Bay and found that for time scales longer than 5 days, the flow was determined by the strength of the Susquehanna River discharge, and wind forcing is important at time scales around 3 days which resulted in a barotropic response. From their analysis of 168 current records from 1973 to 1983, Goodrich and Blumberg (1991) concluded that the typical seasonal wind variability is also a significant influence on the Bay's two-layer circulation, with northerly winds reinforcing the circulation during the winter and southerly winds associated with the Bermuda High acting against the down-Bay surface currents in June–November. Thus, annually recurring wind shifts are a significant factor in setting up the circulation of the Bay.

On shorter time scales, the estuarine circulation's first order seasonality is subject to modulation by episodic atmospheric forcing and subtle influences by the moderate tidal activity that affect the structure of lateral (i.e., cross-channel) currents, residual circulation, and outflow from the Bay's mouth. In a modeling effort using Curvilinear Hydrodynamics in Three Dimensions, Shen and Wang (2007) demonstrated that the dampening of the gravitational circulation by southwesterly

winds is actuated by a significant enhancement of lateral and vertical mixing. These winds also result in a 50% increase in ocean-ward transport time, which has profound implications for export of pollutants discharged into the Bay to the coastal ocean. Further, despite its classification as a microtidal estuary, a recent set of modeling studies has demonstrated clear tidal influences on the Bay's dynamics. Guo and Valle-Levinson (2007) studied the response of Chesapeake Bay to river discharge under the influence and absence of tides with a Princeton Ocean Model-based application and showed that tides reduce the subtidal currents due to greater frictional effects. Using a Chesapeake Bay configuration of the Regional Ocean Modeling System (ROMS), Zhong and Li (2006) demonstrated that 88% of the total tidal energy flux entering the Bay mouth is within the M_2 component and tidal forcing is of equal importance as wind forcing in Chesapeake Bay. In a subsequent application, Li and Zhong (2009) examined flood–ebb and spring–neap variations of turbulent mixing, stratification, and residual circulation in the Bay. They noted a north–south asymmetry in turbulent mixing, coinciding with a clear flood–ebb tidal asymmetry, that they attributed to the phase difference in tidal currents of the upper and the lower Bay. In addition, the spring–neap cycle strongly modulated the turbulent mixing and vertical stratification, and the residual currents during the neap tides were 50% stronger than during the spring tides (Li and Zhong 2009).

The circulation and the salt balance are strongly coupled inside the Bay. The Bay's salt balance is primarily maintained by a longitudinal advective salt flux and a vertical salt flux resulting from mixing. The longitudinal salt flux is mainly driven by the freshwater inputs to the Bay and exchange with the adjacent ocean. Salinity is a major contributor in determining the density structure, which in turn affects the circulation and stratification (Johnson et al. 1991). With near zero salinity for freshwater and near constant salinity for ocean water, salinity structure inside the Bay is an indicator of the exchange at the Bay mouth and the mixing strength.

Understanding of the salinity structure, salinity variability, and the driving force in determining the structure and variability is necessary to advance our understanding of the physical, chemical, and biological dynamics of estuaries. Salinity and its gradient have important ecological impacts. In Chesapeake Bay, salinity influences the distribution, survival, and/or growth of Bay oysters (Calvo et al. 2001; Deksheniaks et al. 1993; Fulford et al. 2007), blue crabs (King et al. 2005; Sandoz and Rogers 1944), clams (Stickney 1964), and submerged aquatic grasses (Orth and Moore 1984). Vertical stratification plays an important role in bottom layer ventilation, which supplies dissolved oxygen to the depths and brings nutrients up from the bottom.

Based on a simple box model approach (Pritchard 1960) and two long-term salinity observation datasets from the Chesapeake Bay Program (CBP) and the Center for Coastal Physical Oceanography at Old Dominion University, Austin (2002) estimated the effective mean exchange rate at the Bay mouth with the coastal ocean and the corresponding salt balance in Chesapeake Bay. Gibson and Najjar (2000) developed a statistical model of the mean salinity for different portions of the Bay using river flow as input to study the salinity change under different climate scenarios. However, the salinity stratification, which is also dependent on the mixing induced by wind, tide, and bathymetry, is more complicated and difficult to predict. A series of fully three-dimensional realizations of the Bay has been developed with the capability of simulating the salinity structure (Guo and Valle-Levinson 2007; Johnson et al. 1991; Li et al. 2005; Wang and Johnson 2000).

The CBP salinity data at the main stem stations were also used in a number of studies to explore the response of the Bay to different forcing. Austin (2004) analyzed the depth averaged mean salinity and salinity difference between 1 and 10 m and found that the variation in both mean salinity and salinity stratification correlated highly with freshwater inputs. Lee and Lwiza (2008) used the observed bottom salinity from 21 CBP main stem stations and identified that the interannual variability of the monthly mean bottom salinity was driven by the freshwater input, while the quasi-decadal variability was associated with non-local forcing through the salt fluxes between the Bay and the ocean. Using Gibson and Najjar's (2000) statistical salinity model, Hilton et al. (2008) found that after removing the signal of the Susquehanna River flow, the residual salinity variability in the Bay correlated with shelf salinity, meridional wind stress, and Potomac River flow.

Despite the detailed theoretical, observational, and modeling studies listed thus far, some important questions about Chesapeake Bay dynamics have not been addressed. In particular, due to the large variability in river load, wind field (both local and far field), surface heat fluxes, and open ocean boundary conditions over seasonal-to-interannual and longer time scales, the relative importance of these forcing mechanisms in driving the Bay dynamics is highly dependent on time scale. Previous modeling studies have focused primarily on relatively short time scales, e.g., on the current structure, the forcing and flow pattern, and basic stratification. Yet the resulting variability in the Bay salinity structure, especially its interannual variability, has not been examined. The studies based on the CBP monitoring data have the advantage of having a long-term time series. However, they were restricted by the data availability and resolution both temporally and spatially.

In addition, the effects of the C&D Canal on Chesapeake Bay dynamics, especially the salinity structure in the upper

Bay, have received little attention. The tidal and subtidal water elevation and flow inside the Canal and their effects on the tidal and non-tidal circulation of the Delaware Bay have been well documented (Najarian et al. 1980; Ward et al. 2009; Wong 1987, 1990, 1991, 2002; Wong and Garvine 1984). However, there have been few detailed investigations on the Chesapeake Bay side and on the salt budget in both systems. Due to the closeness of C&D Canal to the Susquehanna River and greater distance to the ocean on the Chesapeake Bay side, the mean salinity at the Chesapeake end of the canal is typically 2–3 psu lower than that at the Delaware end of the canal (Pritchard and Gardner 1974). Therefore, the subtidal flux-induced salt transport can have a significant role in determining the salinity in the upper reaches of both estuaries.

In this paper, we use a Chesapeake Bay community implementation of ROMS (Haidvogel et al. 2000, 2008; Shchepetkin and McWilliams 2005), which is hereafter referred to as ChesROMS, to investigate the interannual variability of salinity in the Chesapeake Bay. Empirical orthogonal function (EOF) analysis is performed to extract the large-scale spatial patterns with the associated time series, and effort is made to interpret them in the context of physical mechanisms and processes to establish the relationship between the salinity variability and climate forcing.

The paper consists of five sections. The “[Methods](#)” section describes the configuration of ROMS in Chesapeake Bay and the techniques used to validate its output variables. The section “[Model Validation](#)” focuses on model skill assessment. The section “[Climate Forcing and Salinity Variability in Chesapeake Bay](#)” examines the role of climate forcing on salinity variability in Chesapeake Bay using ChesROMS, and the last section summarizes the paper and provides a conclusion.

Methods

ChesROMS Description and Configuration

Figure 1a shows the ChesROMS model grid with bathymetry. The ChesROMS model grid has 150×100 horizontal cells and 20 vertical sigma levels. Inside the Bay and tributaries, the grid sizes vary from 600 to 2,500 m in E–W direction and from 1,500 to 4,500 m in the N–S direction, and the modeled water depth varies from 2 to 35 m. The terrain-following sigma levels are refined in the vicinity of both the surface and the bottom with the vertical s-coordinate stretching parameters (Song and Haidvogel 1994) at the surface and bottom to be 6.0 and 0.95, respectively. Bathymetry data were obtained from the US Coastal Relief Model at the National Oceanic and Atmo-

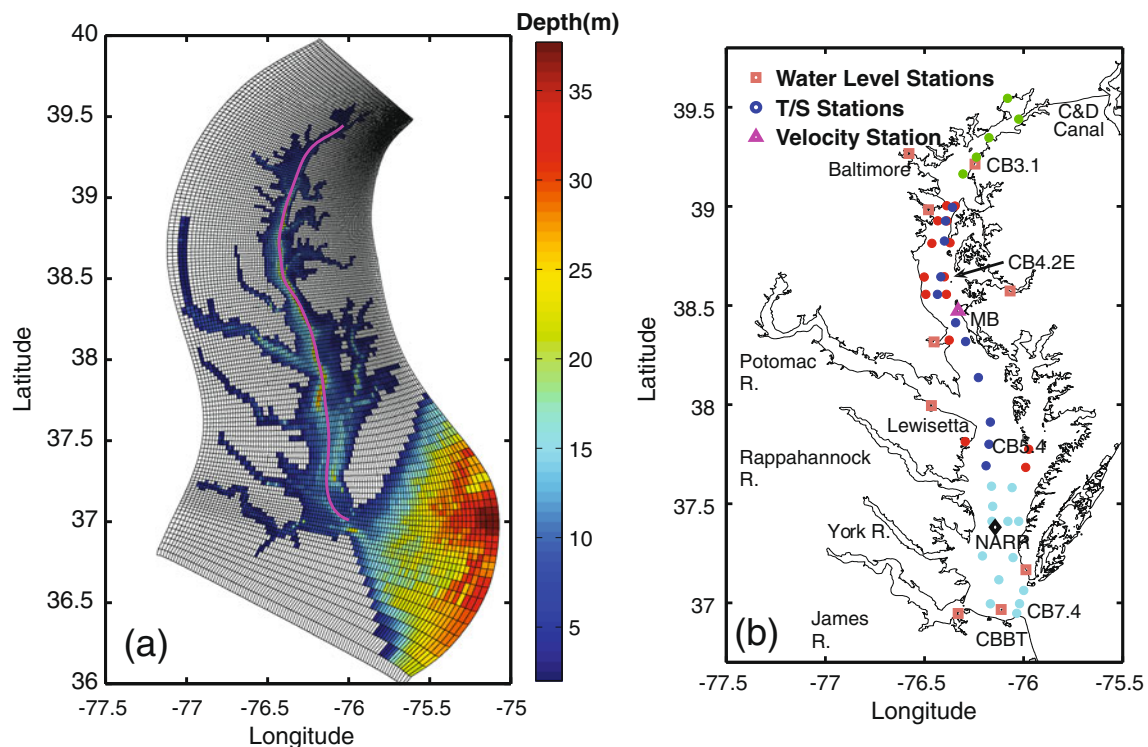


Fig. 1 **a** Model grid and bathymetry of ChesROMS and the location of the longitudinal transect; **b** locations of various datasets

spheric Administration's (NOAA) National Geophysical Data Center.

ChesROMS is forced by open ocean tides and non-tidal water level, river discharge, winds, and heat exchange across the air–water interface. Imposed at the open ocean boundary were nine tidal constituents from the Advanced Circulation Model (ADCIRC) EC2001 tidal database (Mukai et al. 2002), together with non-tidal water levels interpolated from NOAA's tide stations at Wachapreague, Virginia and Duck, North Carolina. Chapman's condition for surface elevation (Chapman 1985) and Flather's condition for barotropic velocity (Flather 1976) were applied to the barotropic component at the open ocean boundary, while for the baroclinic component a radiation condition was used for velocity and a radiation condition with nudging for temperature and salinity. Climatological temperature and salinity from the World Ocean Atlas 2001 was used for nudging (http://www.nodc.noaa.gov/OC5/WOA01/pr_woa01.html) at the open ocean boundary. Daily freshwater discharge data for nine major tributaries (Susquehanna, Patuxent, Potomac, Rappahannock, York, James, Nanticoke, Choptank, and Chester Rivers) from the USGS were applied at the upstream river boundaries, and river temperature was obtained from nearby CBP stations and salinity was set to zero.

Atmospheric forcing, including 3-hourly winds, net shortwave and downward longwave radiation, air temper-

ature, relative humidity, and pressure, was obtained from the North America Regional Reanalysis (NARR) produced at the National Center for Environmental Prediction (<http://www.emc.ncep.noaa.gov/mmb/rrean/>). No assimilation of surface temperature data was performed for the simulations presented here. A series of sensitivity studies were conducted to finalize the model setup. The major conclusions of these experiments are described below.

We experimented with four of the turbulence closure schemes that come with ROMS (Warner et al. 2005b). In our simulations, regular Mellor–Yamada level 2.5 (Mellor and Yamada 1982) and K-profile parameterization (Large et al. 1994) produced similar vertical stratification while $k-\omega$ and Mellor–Yamada level 2.5 implemented using the generic length scale method (Warner et al. 2005b) yielded similar density structures and slightly more stratification in the upper Bay. For results presented here, we used $k-\omega$ as the turbulence closure scheme for better results in the upper Bay.

The model is also sensitive to the background mixing and bottom friction parameters. The background viscosity and diffusivity were set to be 5×10^{-5} and 0.5×10^{-5} m^2/s , respectively, in our final model configuration. The quadratic bottom friction was imposed in the model with a coefficient of 0.003.

We experimented with three different implementations of the C&D Canal by treating it as: (1) an inflow river at different

flow rates, (2) an outflow river at different flow rates, and (3) a tidal boundary. The simulation results indicated that the effect of C&D Canal on the water level in Chesapeake Bay is relatively small. However, the different implementations had a significant effect on the salinity structure, especially in the northern part of the Bay. For the results presented here, we treat the C&D Canal as an inflow river with a constant discharge rate of 350 m³/s. The specified flow rate was well within the magnitude of subtidal flux across the Canal in either direction (Wong 1987) but larger and in the opposite direction of long-term residual flux modeled by Ward et al. (2009). This implementation was selected based on the modeled salinity calibration in the upper Bay. Both temperature and salinity values from the CBP station at Chesapeake City (CC) were used in setting the boundary conditions, which is different from the other river boundaries described above. The inflow flux together with the salinity at CC (which varies from 0 to over 10) results in a net salt flux into Chesapeake Bay.

Freshwater transports are imposed at the head of each major river. The flow rates are taken from USGS gauges below the fall lines. The gauged flow was adjusted according to Table 1 to reflect the runoff contributed by tributary drainage areas downstream of the gauged stations. Table 1 was created according to Thatcher and Najarian (1983) and Seitz (1971) except for the Patuxent River and the Northern branch of the James River. For these two tributaries, we obtained the gauged area directly from the USGS because we used different stations in our study. No adjustments were made to the Nanticoke River and the Chester River. In part, this is due to their small contributions to total discharge but is also due to the considerable discrepancy in the gauged area between the above studies

Table 1 List of river basins and the factors for adjusting the freshwater discharge based on total drainage area of each river basin and the gauged area of the stations

River basin	USGS gauge station	Gauged area (mi ²)	Total area (mi ²)	Ratio
Susquehanna	01578310	27,483	27,496	1.0
Patuxent	01594440	348 ^a	882.4	2.536
Potomac	01646500	11,560	13,920.8	1.204
Rappahannock	01668000	1,599	1,008.8	0.631
York Pamunkey	01673000	1,072	1,459.9	1.362
Mattaponi and Lower York	01674500	619	1,148.7	1.856
James Northern Branch	02035000	6,257 ^a	6,989.9	1.117
Appomattox and Lower James	02041650	1,335	3,164.8	2.371
Choptank	01491000	140.9	760.3	5.396

^a Gauged area obtained directly from USGS

and the USGS website. The ungauged freshwater runoff was estimated to be about 10% of the gauged discharge into Chesapeake Bay. These adjustments do not have a significant effect on the circulation and salinity in the main stem of the Bay. However, they are retained within the model configuration because of the significant impacts they are likely to exert on the biogeochemical cycles that will be targeted in future studies. The development and final configuration of the model are documented and available as an open source distribution for the oceanographic research community (<http://sourceforge.net/projects/chesroms/>).

Validation Methods

The following analyses were performed to evaluate the skill of ChesROMS model results.

Tidal Harmonic Analysis

The modeled and observed water levels consist of both tidal and non-tidal components. Least square harmonic analysis (Foreman 1977) was performed on both datasets to estimate the amplitudes and phases of selected tidal constituents. The harmonic constants were compared directly against each other for the tidal validation and were also used to reconstruct the tidal water elevation. The non-tidal component was defined to be the residual of the total water level less the tidal component.

Time Series Comparison

Most observations were available as time series at specific sites. These time series were compared against model results interpolated to the same location. For water level and currents, the tidal components can be removed either by harmonic analysis or low pass filtering so that subtidal signals can be compared. Time series data were also used for point-to-point comparison in scatter plots and calculating statistical measures of model performance as described below.

Statistics and Taylor Diagrams

Direct point-to-point comparisons were made between the observations and the model by sampling the model results to the same horizontal, vertical, and temporal locations as the time series data. Mean and standard deviation of both modeled and observed fields were compared, and root mean square error (RMSE), correlation coefficient (*R*), model skill (MS) (Li et al. 2005; Warner et al. 2005a; Wilmott 1981), and skill score (SS) (Allen et al. 2007; Murphy 1988; Oke et al. 2002; Ralston et al. 2010) were calculated for each variable (temperature,

salinity, and water level). The MS and SS are defined as follows:

$$MS = 1 - \frac{\sum |X_{\text{model}} - X_{\text{obs}}|^2}{\sum \left(|X_{\text{model}} - \bar{X}_{\text{obs}}| + |X_{\text{obs}} - \bar{X}_{\text{obs}}| \right)^2}$$

$$SS = 1 - \frac{\sum |X_{\text{model}} - X_{\text{obs}}|^2}{\sum \left(|X_{\text{obs}} - \bar{X}_{\text{obs}}| \right)^2}$$

Standard deviation, correlation coefficient, and the centered pattern or unbiased RMSE (RMSE') were collectively summarized using Taylor diagrams (Taylor 2001) (e.g., Fig. 2), where the radial distance from the origin represents the standard deviation of the modeled field; the azimuthal position conveys the correlation between the two fields; and the RMSE' of the modeled field is proportional to its distance to the observed point (in the same unit as the standard deviation). When the standard deviation is normalized by the observed standard deviation, the observation will always be at a point with unit distance from the origin along the abscissa (normalized standard deviation=1, correlation=1 and RMSE'=0), shown as the black circle in Fig. 2. The normalization also allows different variables to be summarized in the same diagram. The drawback of the normalization is that only the relative magnitude of the model/data variability is shown and the absolute values of the RMSE' are also expressed in proportion to the observational data variability. Note that the information shown in a Taylor diagram does not include the bias of the modeled field, i.e., the difference in the means between the modeled and observed field. However, we examine RMSE, which includes both RMSE' and bias, as well as the direct comparison of the means in the detailed skill assessment (e.g., Table 2).

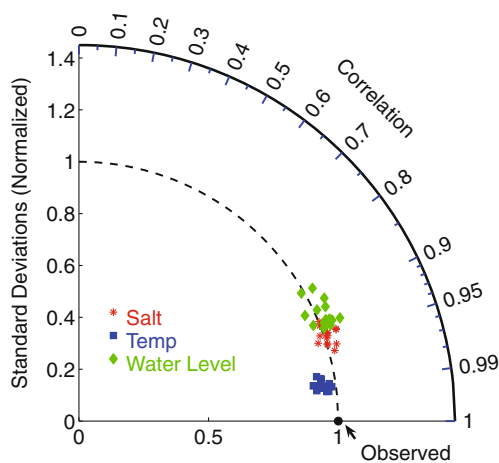


Fig. 2 Taylor diagram showing the normalized standard deviations, correlations and RMSE' of water level (green diamond), temperature (blue square), and salinity (red star) for years 1991–2005. Each point in one variable group corresponds to model skill assessment over a year

Model Validation

Overall Model Skill

The model was run for 15 years from 1991 to 2005, 1 year at a time. The first year simulation started with meridionally varying temperature and salinity and was spun up from rest for a year and the consecutive years were hot restarted, i.e., the year-end conditions of the previous year were taken as initial conditions for the next year. Model results were saved hourly at specified stations for the model validation and daily for the whole grid.

The annual mean river discharge into Chesapeake Bay for 1991–2005 (Fig. 3) shows significant interannual variability. The high/low flows and the average that occurred during this 15-year period are comparable to the high/low and average river discharge values in the long-term record since 1937. Therefore, the modeled period is also representative of the longer-term variability in the region.

ChesROMS captures the overall and annual variability of the simulated fields of temperature, salinity, and water level very well. Overall and annual performance statistics for the 15-year period (1991–2005) of these variables are listed in Table 2 and displayed in Fig. 2, respectively. In the Taylor diagram (Fig. 2), each point represents 1-year's model results contrasted against all available observations (details on the data source and availability will be discussed in following subsections). Temperature was most consistently well predicted, with correlation around 0.99, and a RMSE of 1–1.5°C (Fig. 2, Table 2).

For water level, the agreement between modeled and observed tidal component is better than the non-tidal water elevation, which can be affected by both local and far-field wind forcing (Table 3). Note that the statistics are performed on exact point-to-point comparisons, where the errors in water level predictions consist of mismatches in both amplitude and phase. Nonetheless, the correlation coefficients between modeled and observed water level were typically greater than 0.9 and the RMSEs were between 10 and 20 cm with all storm events included. The seemingly lower overall model skill of water level prediction compared to temperature and salinity can be attributed to: (1) higher sampling frequency for comparison (hourly vs. biweekly) and (2) fewer stations and most locations near the shoreline or inside tributaries (Fig. 1b).

Though salinity in the Bay undergoes considerable year to year variability that depends primarily on freshwater discharge, ChesROMS performed similarly well for all years on a Bay-wide scale and no systematic pattern could be observed for different years (Fig. 2). The modeled salinity correlated well with observations (correlation coefficient around 0.95) and RMSE was about 2–2.5

Table 2 Model performance evaluation for the whole time period of 1991–2005

Variable	Modeled		Observed		RMSE	MS	<i>R</i>	SS
	Mean	Std	Mean	Std				
Water level (m)	0.08	0.30	0.04	0.29	0.13	0.95	0.91	0.80
Temperature (°C)	16.41	7.51	16.70	7.93	1.28	0.99	0.99	0.97
Salinity	17.12	6.71	16.83	6.63	2.28	0.97	0.94	0.88

Measures listed are: modeled mean, modeled standard deviation (Std), observed mean, observed standard deviation, root mean square errors (RMSE), model skill (MS), correlation coefficient (*R*), and skill score (SS)

(Fig. 2 and Table 2). All annual points in the salinity group are located close to one another and the dashed line (Fig. 2), which indicates that the modeled and observed salinity variability compare favorably when all stations are considered together. Greater variation in observed salinity was apparent, however, when comparisons are performed at individual stations, as will be shown later in the section “Salinity Validation Under Contrasting River Forcing”.

To examine model performance on an intra-annual and at a spatially dependent scale, we present results in the following sections of a comparison between simulated and observed water level, currents, and temperatures in a year (1998) of typical freshwater discharge (Fig. 3), and for salinity in years of low, normal, and high river outflow at locations throughout the main stem of Chesapeake Bay.

Water Level Validation in 1998

Hourly water level observations were obtained from NOAA’s Center for Operational Oceanographic Products and Services (<http://tidesandcurrents.noaa.gov>). The station locations are marked in Fig. 1b. Both observed and modeled water levels were decomposed into tidal and non-tidal components.

The water level time series are depicted in Fig. 4 at three selected stations: Baltimore, Lewisetta, and the Chesapeake

Bay Bridge Tunnel (CBBT) (Fig. 1b). The water level prediction (both amplitude and phase) was generally better in the lower Bay than in the upper Bay. The RMSEs of tidal water elevations are 5.7, 3.6, and 3.0 cm for Baltimore, Lewisetta, and CBBT, respectively. The model skill of tidal elevation for the three stations was 0.98, 0.99, and 0.99, respectively. Table 3 lists nine tidal constituents analyzed from both the modeled and observed water levels (see “Tidal Harmonic Analysis”) at CBBT at the Bay mouth. For each tidal constituent, the amplitude error was within 1.2 cm and phase error within 1.5 h. However, it was noted that at CBBT, the M_2 tide alone could contribute an error of up to 7 cm when errors in both the amplitude and phase (Table 3) were combined. Experiments of tuning the tidal components on the open boundary obtained from the ADCIRC database based on the mismatch of major tidal constituents at CBBT effectively improved the model–data tidal comparison at CBBT and the improvements propagate into the interior of the Bay. However, this approach was not adopted here because it cannot be readily applied in forecasting without data assimilation. Nonetheless, it points out the necessity of a more accurate tidal database to provide better open boundary conditions to estuarine and coastal models.

The errors in non-tidal water elevation, hence in full water level that consists of both the tidal and non-tidal components, are generally greater because the prediction of non-tidal water level involves more processes, such as the baroclinic density structure and remote and local wind forcing. The RMSE for the total water elevation in 1998 was 13.0, 9.8, and 9.6 cm at Baltimore, Lewisetta, and CBBT, respectively.

Velocity Validation in 1998

Continuous, 5-min resolution current meter data were collected from 1988 onward by two fixed buoys that are part of the Chesapeake Bay Observing System (CBOS). We present the comparison between modeled and observed velocity at the mid-Bay (MB) station (Fig. 1b). At MB, currents are measured at two fixed depths—2.4 and 18.9 m.

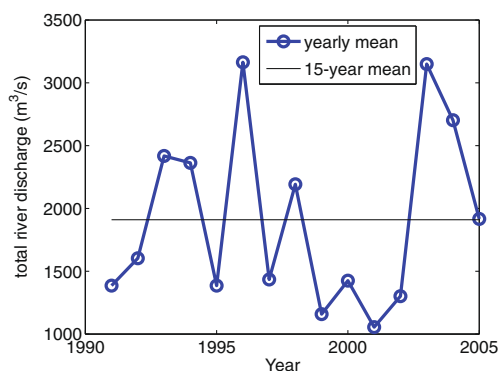


Fig. 3 Total river discharge (cubic meter per second) from nine major tributaries into Chesapeake Bay in 1991–2005

Table 3 Modeled and observed amplitudes (in meters) and phases (in hours) of nine tidal constituents at Chesapeake Bay Bridge Tunnel

Tide	Period	Mod_amp	Mod pha	Obs_amp	Obs pha	Err_amp	Err pha
M ₂	12.4206	0.3999	5.8912	0.3883	-6.1613	0.074	12.0525
S ₂	12.0000	0.0796	1.0166	0.0671	1.5714	0.025	-0.5547
N ₂	12.6583	0.0989	3.1183	0.0893	3.3452	0.014	-0.2268
K ₁	23.9345	0.0576	11.8988	0.0459	12.1670	0.012	-0.2682
M ₄	6.2103	0.0072	-2.4682	0.0057	2.9293	0.005	-5.3975
O ₁	25.8193	0.0370	-0.0842	0.0366	1.0804	0.010	-1.1646
M ₆	4.1402	0.0055	0.4426	0.0062	0.6502	0.002	-0.2076
Q ₁	26.8684	0.0083	-6.9615	0.0094	-5.6701	0.003	-1.2913
K ₂	11.9672	0.0149	-5.0348	0.0140	-4.9052	0.001	-0.1295

The amplitudes of error have taken into account the difference in both the amplitudes and phases of each constituent

Model results from the cell where the station is located are interpolated to the same depths, and the along-Bay velocity components are plotted together with the observations for the period of day 300–330 in 1998 (Fig. 5). Positive values correspond to landward flows, i.e., toward the head of the Bay. Also shown are the longitudinal winds from NARR and CBOS (Fig. 5a). During this period, a prolonged (ca. 10-day) period of calm to medium northerly winds was followed by a strong southerly wind event and subsequently alternating northerly and southerly wind events. The 3-hourly NARR winds (red dashed line) that were used as the model's surface forcing agree well with the observed CBOS winds, though with some underestimation of the magnitude and noticeable smoothing effects because of coarser time resolution. The instantaneous currents display a strong tidal signal with pronounced wind modification under strong wind conditions (e.g., days 313–315).

The subtidal velocity for the same time period was obtained by passing both the observed and modeled currents through a low pass filter (Fig. 6). Under calm wind conditions (days 304–312), the currents in the mid-Bay displayed the typical two-layered gravitational circulation (Hansen and Rattray 1965; Pritchard 1952), with the upper layer flowing seaward and the lower layer flowing up the Bay. However, the strong southerly wind event around days 313–314 completely reverses the subtidal circulation by forcing the surface layer to flow northward and the pressure setup against the Bay head results in a seaward bottom layer flow, which lags the surface response by about 1 day. Following this, the relaxation of the strong southerly winds and subsequent northerly winds force the surface water to speed southward again, which consequently resulted in the reestablishment of a strong bottom return flow. Thus, the two-layer gravitational circulation was

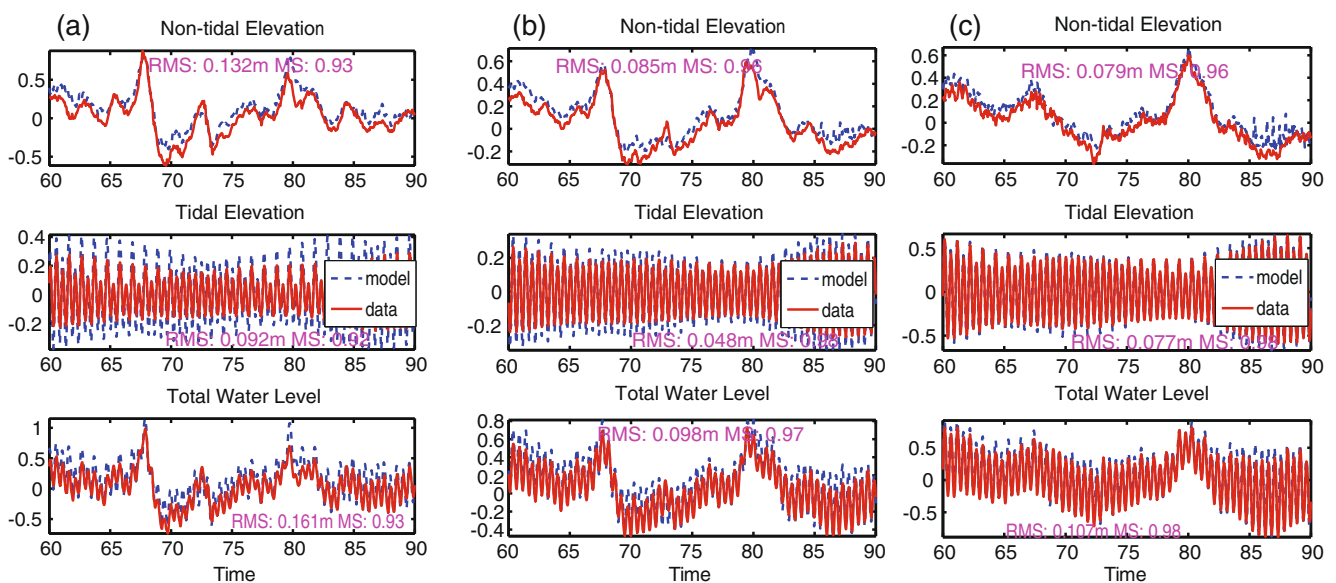


Fig. 4 The water level time series in October 1998 at three selected stations: **a** Baltimore, **b** Lewisetta, and **c** CBBT

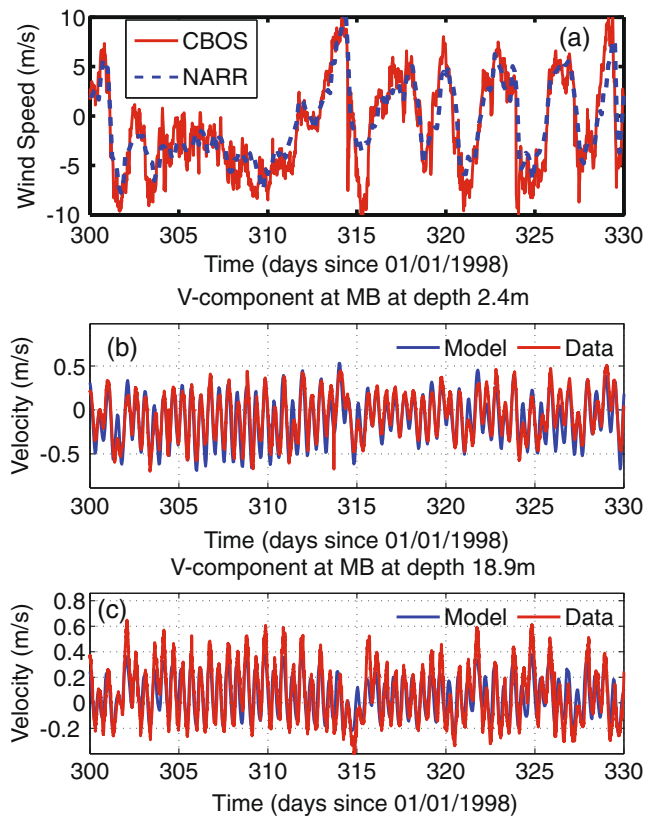


Fig. 5 The along-Bay component of **a** wind from CBOS and NARR and current velocity from observation (*red line*) and model (*blue line*) at CBOS station MB at **b** 2.4 m and **c** 18.9 m. Positive values correspond to north/landward velocity

enhanced with the bottom layer response to the surface forcing again lagging the surface layer by about 1 day. The modeled currents generally match the observed flow pattern. However, the lower layer currents in the model are somewhat damped compared to observations. We suspect that the grid resolution plays an important role in the underestimation of bottom layer currents, i.e., the inherent smoothing associated with the coarse grid results in a shallower main stem channel that very likely restricts and dampens the deep flows. For example, at the MB station, 18.9 m depth in the model is roughly 2 m above the bottom, while in reality it is positioned approximately 9 m above the bottom. To explore this conjecture, the modeled along-Bay current at 12 m depth (i.e., 9 m above the model bottom level) was also plotted in Fig. 6b (dashed line) and showed a much stronger correspondence in magnitude to the observed bottom current.

Temperature Validation in 1998

Temperature (and salinity) observations at over 100 stations distributed throughout the Bay are available from the Chesapeake Bay Monitoring Program. At each station, a

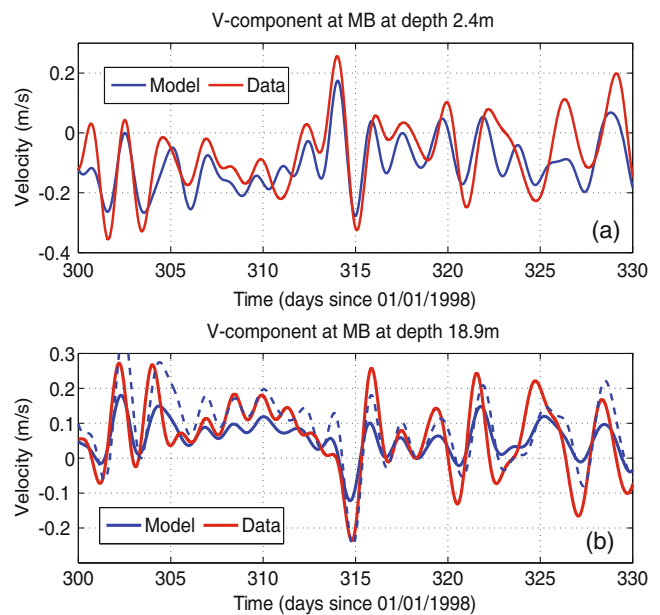


Fig. 6 Same as Fig. 5 but with low pass-filtered velocity. The dashed *blue line* in **b** is modeled v-component velocity at 12 m (approximately the same distance to the bottom as the observation)

vertical profile of measurements is taken once or twice a month at somewhat irregular time and depth intervals, usually with more frequent measurements taken from spring to autumn. To compare the model with the observations directly, we sampled the model results at the same time, location, and depth as the field measurements.

The skill of the model's simulation of temperature at all available stations (ca. 40 stations) in the main stem of the Bay in 1998 is summarized in a Taylor diagram (Fig. 7), where each point represents one station. The stations are further divided into four spatial groups: upper Bay, mid-Bay channel, mid-Bay flanks, and lower Bay (Fig. 1b). At all stations, the modeled temperature matched the observations with correlation coefficient generally greater than 0.99, denoting a remarkable agreement in the phasing of model simulated temperatures to observations; RMSEs are correspondingly less than 1.5°C. Temperature measurements from one station from each of these spatial groups—CB3.1, CB4.2E, CB5.4, and CB7.4—were chosen to represent the attendant regime (Fig. 1b).

Figure 8 shows the time series of temperature profiles at these four stations. To condense the vertical and temporal information into one comparison, at each time (the *x*-axis), both modeled and observed values along the entire vertical profile were plotted side by side using different symbols, with symbol size relating to the sample depth (i.e., larger size for increasing depth). These comparisons illustrate the model–data correspondence and particularly emphasize the agreement in temporal evolution of vertical stratification. Temperature in Chesapeake Bay has a clear seasonal cycle

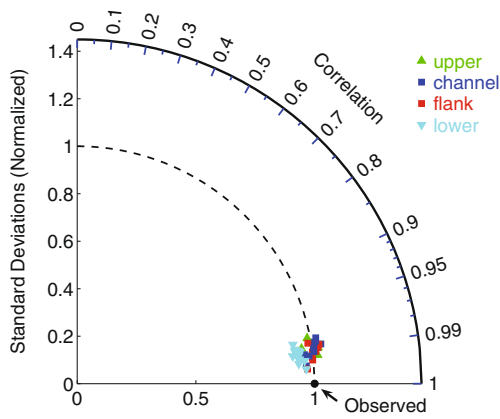


Fig. 7 Taylor diagram of temperature at each station in 1998. Each point represents the comparison of time series of vertical temperature profile at one station over the year

with values typically ranging up to 28°C in summer and down to ~0°C in winter (not shown). Due to the influence of the strong 1997/1998 El Niño event (Dong et al. 2000; Grötzner et al. 2000), the observed water temperature in 1998 in the main stem did not drop below 5°C. The horizontal temperature gradient is relatively small with a slightly warmer lower Bay in winter and a cooler lower Bay in summer. Moreover, the vertical temperature stratification is usually minimal in fall and winter due to vertical mixing

induced by surface cooling and stronger winds. Maximum thermal stratification generally occurs during the spring–summer transition due to surface heating and calmer winds. RMSE for temperature is less than 1.5°C and the MS is ≥ 0.99 for each of the stations shown (Fig. 8). The corresponding point-to-point comparisons are also shown in Fig. 9, with high correlations (≥ 0.99) between modeled and observed temperature at each station. The step-like behavior at CB3.1 (Fig. 9) is mainly due to the mismatch between the modeled and observed depth (approximately 7 vs. 13 m). For the point-to-point comparison, we simply repeated the bottom value when observed depth is greater than the bottom depth in the model. In addition, the less stratified dataset will align perpendicularly to the corresponding axis because of its similar values.

Although active meteorological forcing is used, ChesROMS reproduces Bay-wide temperature very well. This is in contrast to Li et al. (2005) in which nudging to observed sea surface temperature was used. This is encouraging for the use of ChesROMS for Bay-wide forecasting when no measurements are available for nudging.

Salinity Validation Under Contrasting River Forcing

Accurate simulation of the Bay’s salinity distribution is more of a challenge because it is affected by freshwater

Fig. 8 Observed (red asterisk) and modeled (blue circle) temperature in 1998 at **a** CB3.1, **b** CB4.2E, **c** CB5.4, and **d** CB7.4 (from upper to lower Bay). Each vertical group of symbols represents a vertical profile at the corresponding time. Size of the symbols is coded by depth with bigger symbols for greater depth

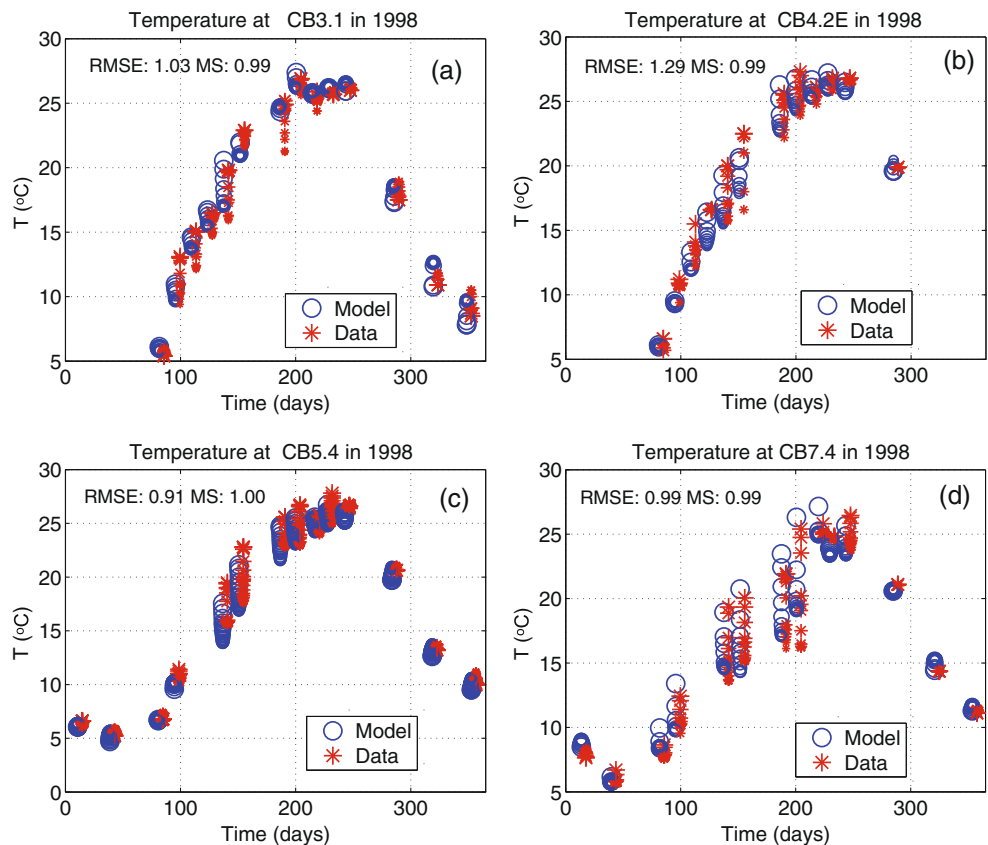
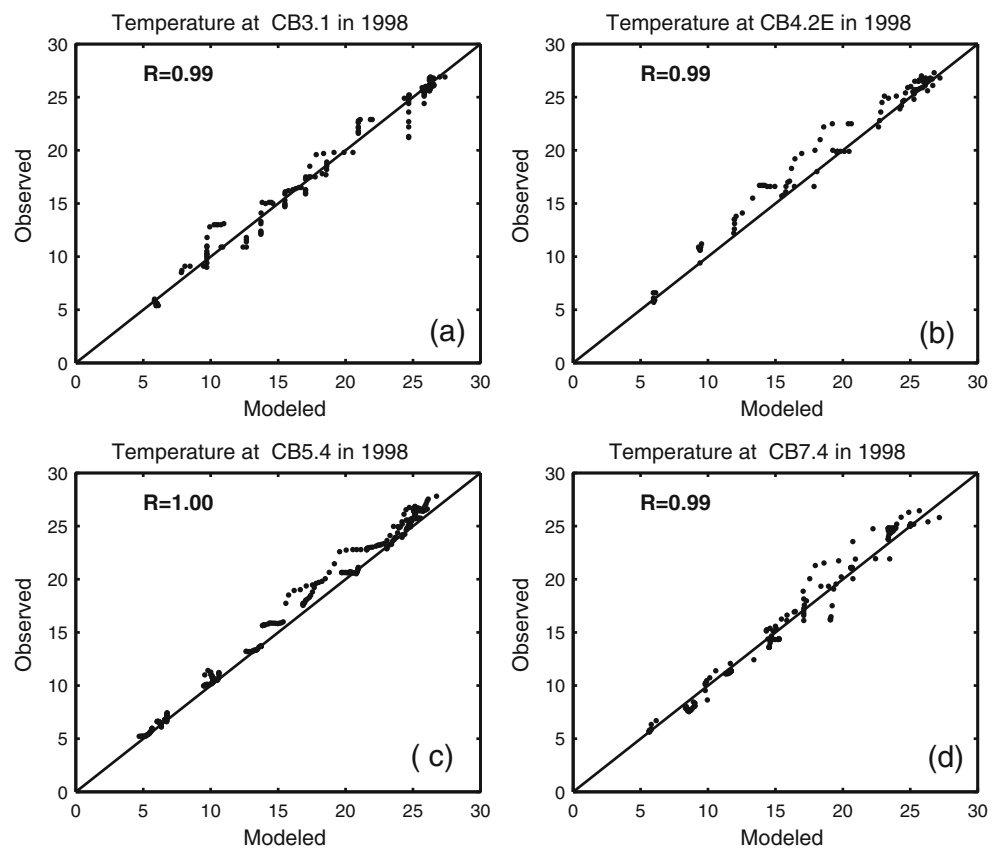


Fig. 9 Modeled vs. observed temperature in 1998 in scatter plot at the same locations as in Fig. 8: **a** CB3.1, **b** CB4.2E, **c** CB5.4, and **d** CB7.4



loading, open ocean boundary conditions, advection, mixing, and the net effect of precipitation and evaporation. Because of the large difference between the Bay's two end members (fresh riverine waters with salinity at 0 and ocean water with salinity at about 35), a small change in circulation and mixing can significantly affect salinity structure. As characterizing salinity variation in Chesapeake Bay is a focal point of this paper, and because river discharge plays a primary role in determining salinity structure in the Bay, the model's performance in dry (2001), normal (1998), and wet (2003) years are examined in detail for a more complete assessment of model performance under different freshwater forcing conditions.

The statistics of model skill in salinity at each main stem station are summarized in Taylor diagrams (Fig. 10) and listed in Table 4 for all the stations. The mean salinities in these 3 years clearly reflect the influence of river discharge with relatively high salinity in 2001 and low salinity in 2003 (Table 4). Bay-widely, the modeled salinity captures the observed mean and variation very well (Table 4). Correlations between modeled and observed salinity are greater than 0.7 at most stations in all three representative years (Fig. 10). The modeled salinity generally exhibited less variability than the observations, especially in the mid reach of the Bay over the deep channel. However, the modeled salinity occasionally displayed a greater variance (shown as the stations that fall outside of the dashed line in

Fig. 10) in the mid to lower reach of the Bay over the flanks. The station in Fig. 10c with nearly zero correlation with observations is located near the Susquehanna River mouth. In 2003, the station remained fresh throughout the year except during and after Hurricane Isabel, when the bottom salinity reached nearly 3. The model reproduces nearly zero salinity there and captures the salinity surge during the event but the effect lasts for a shorter period of time (not shown). Apparently, correlation and MS calculations are not effective measures of skill under such conditions with a nearly constant variable. This problem was also apparent at another fresh station, i.e., CB1.1 (see Table 5 in the Appendix).

Note that the model skill for salinity is considerably better when considering all stations together (Fig. 2 and Table 4) than at individual stations (Fig. 10 and Table 5), which is in contrast to the temperature model skill (Figs. 2 and 7). For temperature, the main controlling process is the seasonal cooling/warming, which is reproduced well at each station. The spatial difference is relatively small and secondary. However, the first order characteristic of the salinity structure in the Bay is the large horizontal gradient that results from advection, which cannot be well presented by the point-to-point comparison at one station. The model captures the large-scale spatial pattern very well but often shows relatively large error in salinity at specific stations and times.

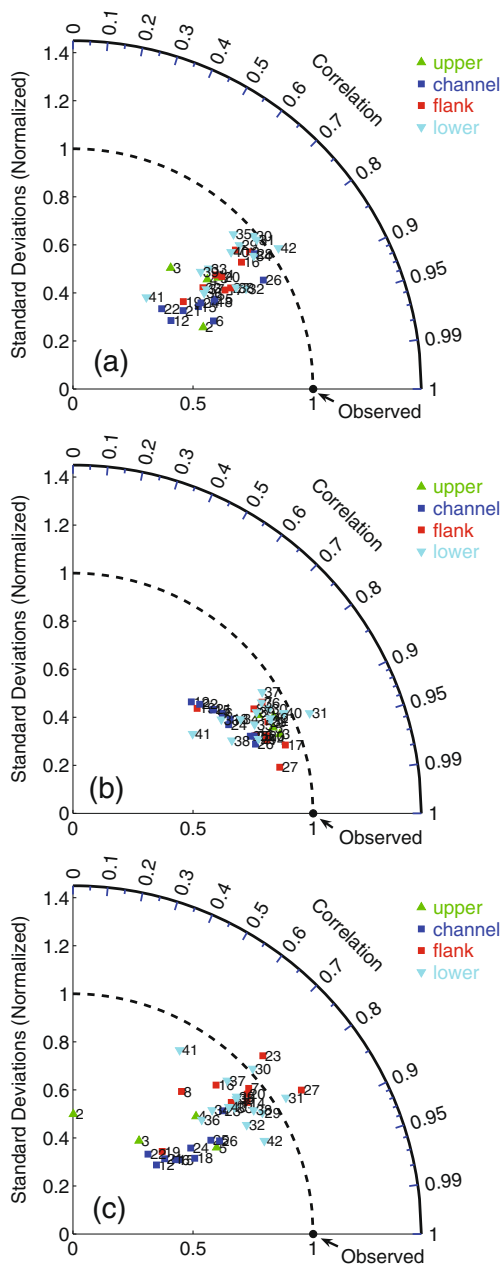


Fig. 10 Same as Fig. 7 but for salinity in **a** 2001 (dry), **b** 1998 (normal), and **c** 2003 (wet) years

Salinity structures at the four stations examined above for temperature—CB3.1, CB4.2E, CB5.4, and CB7.4—displayed a seasonal cycle in both salinity values and stratification in 1998 (Fig. 11). Salinity is at its lowest in spring and at its highest in late fall/winter, following the fresh water discharge cycle. Stratification, however, is usually highest in late spring due to large freshwater input and lowest in fall because of low freshwater input and strong wind mixing. Modeled salinity structures generally followed the observations closely. However, in the upper Bay, modeled bottom salinity usually did not reach as high values as in the observations (Fig. 11a), and in the mid-Bay over the shoals, modeled salinity was generally higher than the observations (Fig. 11b). The scatter plots for the four stations illustrate the relatively high correlation in the point-to-point comparisons and the same overestimation bias in mid-Bay stations, i.e., CB4.2E and CB5.4 (Fig. 12). The statistics at all main stem stations in 1998 as well as in 2001 (dry year) and 2003 (wet year) are listed in Table 5 in the Appendix. The examination of model results from other years leads to very similar salinity structures and model–data agreement (not shown).

Climate Forcing and Salinity Variability in Chesapeake Bay

Forcing and Salinity Climatology in Chesapeake Bay

In this section, we describe the climatology of the salinity field and major forcing of the Chesapeake Bay dynamics. The climatology in the study refers to the corresponding mean of the model forcing and the modeled salinity field over the 15-year period from 1991 to 2005.

River Discharge

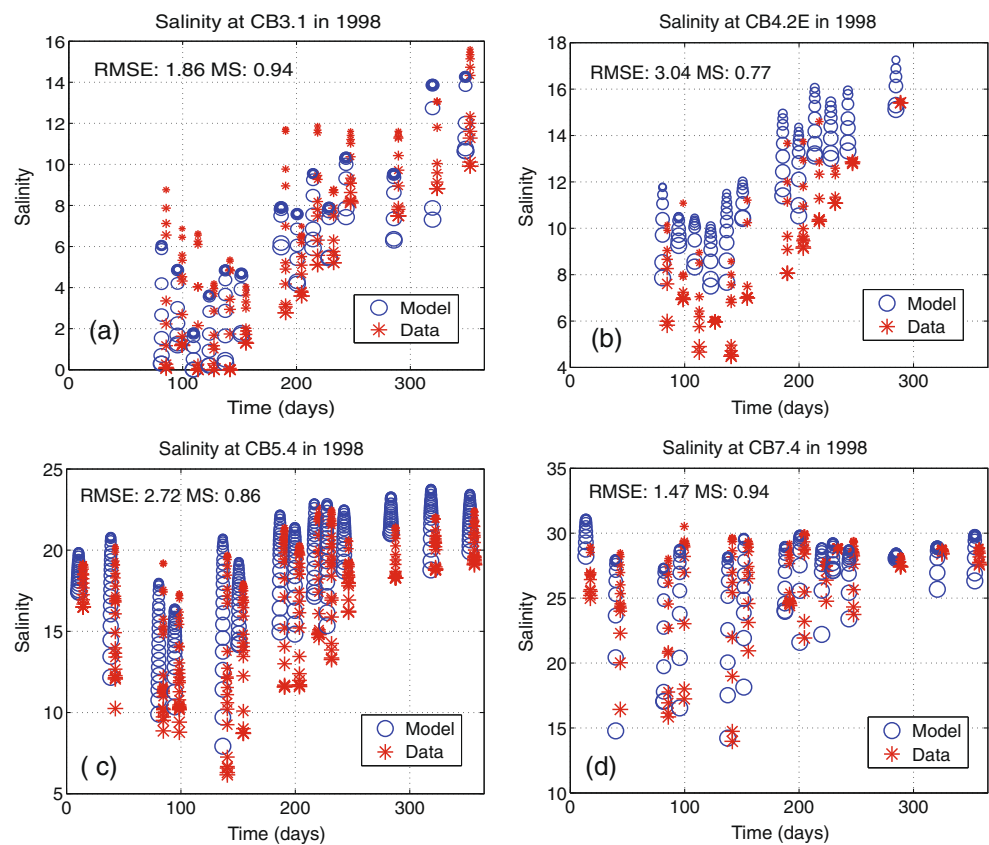
The total river discharge into Chesapeake Bay varies greatly from year to year (Fig. 3). However, the climatological total freshwater discharge into the Bay displays a distinct seasonal pattern: it is highest in spring due to

Table 4 Model performance evaluation for salinity at all main stem stations in 1998, 2001, and 2003

Year	Modeled		Observed		RMSE	MS	R	SS
	Mean	Std	Mean	Std				
1998	16.43	6.77	15.23	6.71	2.49	0.97	0.95	0.86
2001	18.80	6.26	18.14	6.24	1.99	0.97	0.96	0.90
2003	15.03	6.50	14.81	6.49	2.55	0.96	0.92	0.85

Measures listed are: modeled mean, modeled standard deviation (Std), observed mean, observed standard deviation, root mean square errors (RMSE), model skill (MS), correlation coefficient (R), and skill score (SS)

Fig. 11 Same as Fig. 8 but for salinity **a** CB3.1, **b** CB4.2E, **c** CB5.4, and **d** CB7.4



snowmelt inputs, lowest in summer and increases somewhat in the fall/winter depending on the amount of precipitation (Fig. 13a). Even though Fig. 13a shows only the aggregated river discharge into the Bay, all major individual rivers display a similar climatological seasonal pattern, with a slight time lag for the Susquehanna River reaching maximum river flow because of its higher latitude.

Wind

Figure 13d–f illustrates the climatology of wind forcing from NARR at one grid cell over the mid to lower Bay (cell location shown in Fig. 1b). Wind speed is usually low in summer and high in winter and spring (Fig. 13f). In winter and spring, the along-Bay (N–S) winds typically blow from the north (negative), while in summer they are generally southerly (positive) (Fig. 13e). The cross-bay (E–W) wind is strong and toward the east (positive) in winter and spring, while generally weaker in summer (Fig. 13d).

Salinity

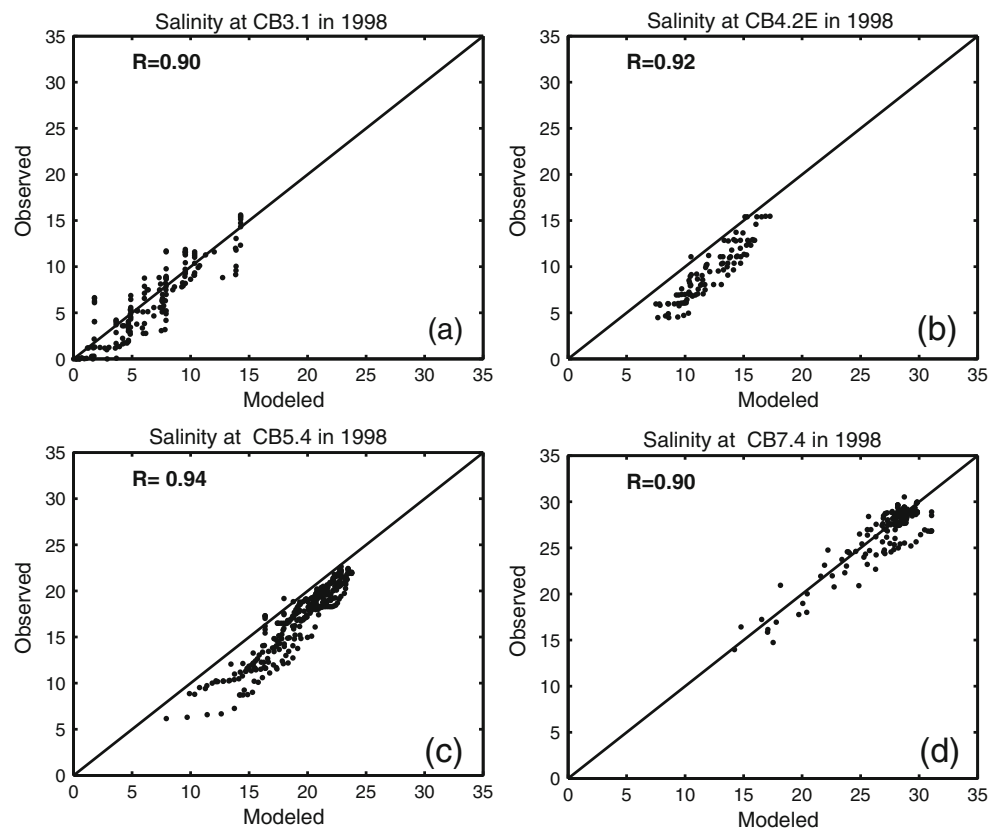
The climatology of Bay-wide averaged surface, bottom, and depth integrated (not shown) salinity follow the same pattern (Fig. 13b), with surface salinity displaying greater high-frequency variation. Bay-wide mean salinity is at the lowest in late spring and at the highest in fall. Surface

salinity varies by 3.5 seasonally and bottom salinity varies by 2.5 on average. River discharge is the dominant forcing in determining total salinity in Chesapeake Bay with an obvious inverse relation between salinity variation in the Bay and the freshwater input. However, the Bay responds to river discharge on differing time scales that are dependent on the rate of river discharge. During peak river discharge (spring), the Bay-wide surface salinity minimum (at around day 132) lags the river discharge maximum (at around day 89) by about 40 days, whereas during low river discharge (summer/fall), Bay-wide surface salinity reaches its maximum (at around day 314) about 70 days after minimum river discharge occurs (at around day 242). Therefore, the mixing time of the Bay is longer when river discharge is low and vice versa. Various studies (Kranenburg 1986; Lerczak et al. 2009; Maccready 1999, 2007) have indeed shown that the response time of an estuary scales with the advective time scale which will result in a shorter response time during peak river discharge.

The high-frequency variation in surface salinity indicates that the surface water also responds to rapidly changing surface forcing, but the effect is less pronounced in the bottom layer, especially in the spring. However, winds can affect the bottom layer in fall by seasonally eroding stratification.

The stratification indicated by the bottom and surface salinity difference also displays a seasonal cycle that

Fig. 12 Modeled vs. observed salinity in 1998 in scatter plot at the same locations as in Fig. 11: **a** CB3.1, **b** CB4.2E, **c** CB5.4, and **d** CB7.4



coincides with the high-frequency variation in the surface salinity (Fig. 13c). The stratification is generally high in summer and low in fall and is clearly inversely related to the wind speed with a strong modulation by the effect of river discharge (Fig. 13c, f, a). High river discharge can intensify the stratification as well as induce mixing from the large velocity shear. The variation in the salinity stratification demonstrates the complex balance between river discharge, tides, and winds in determining the salinity structure in the system.

Salinity Variability in Chesapeake Bay

To examine the salinity variability in Chesapeake Bay, we calculated the 2-day mean over each grid cell of the modeled salinity and performed an EOF analysis on the anomaly of each cell (by removing the climatology discussed above) over the 15-year period (1991–2005). The 2-day averaging period was chosen solely due to computational constraints compared to the analysis of the original daily averaged field. However, the 2-day averaging is sufficient for our focus on exploring longer-term salinity variability in the Bay. Furthermore, we repeated the EOF analysis along the longitudinal transect discussed in the section “Salinity Variability Along the Longitudinal Transect” based on the daily anomaly to test the effect of 2-day averaging period on the analysis results. In all of the

following EOF discussion, the maps show the spatial pattern while the time series show the temporal evolution of the salinity field. Spatiotemporal salinity variations in these EOFs can be reconstructed via the product of the magnitude at a given location and the time series value at a given time.

Surface and Bottom Salinity

Nearly 80% of the total variance in both surface and bottom salinity can be explained by their first EOF modes (Fig. 14). Between the surface and bottom salinity, there is a strong similarity in the magnitude of the first mode, as well as its spatial and temporal patterns. The salinity can deviate by up to 10 from the mean state in the Bay. The areas with the highest variability are downstream of the freshwater sources in the mid- to upper Bay in the main stem and the middle reaches of the tributaries. At the river and Bay heads, the variation is zero because the water in these areas is always fresh. The bottom salinity exhibits little variation near the Bay mouth because climatological salinity was used at the open boundary and bottom water in this region usually possesses relatively high salinity. At the bottom, salinity variation is generally less than at the surface, except in the upper Bay and mid to upper tributaries where salinity fronts are located. The changes in the strength of the two-layer circulation determines the extent of the salt intrusion in the bottom layer and drives

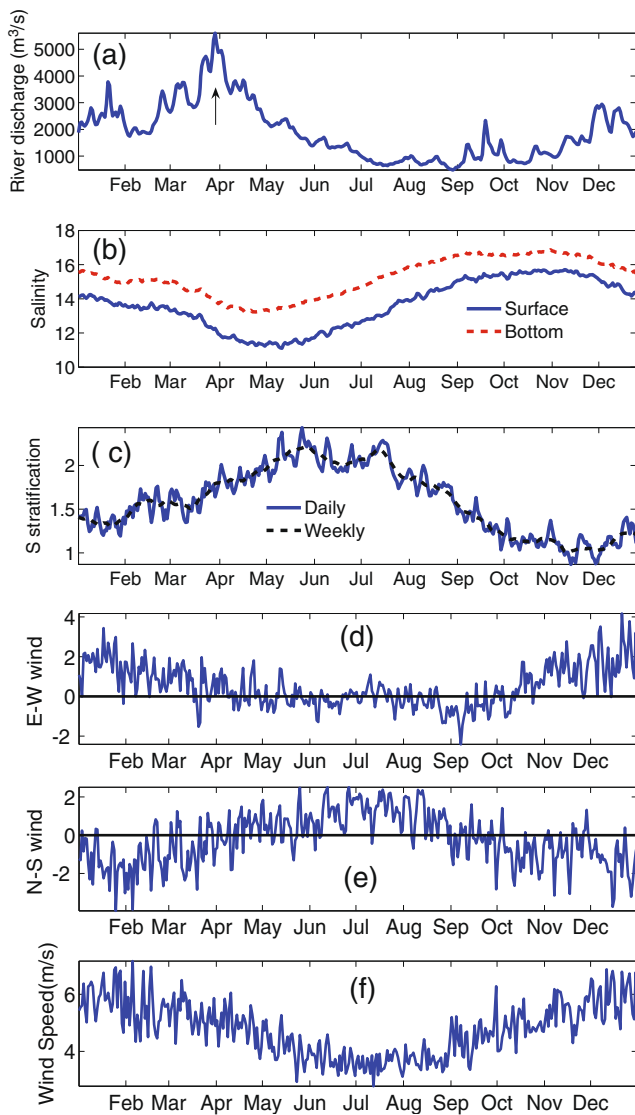


Fig. 13 Climatology of **a** river discharge, **b** Bay-wide surface and bottom salinity, **c** salinity stratification, **d** E–W wind, **e** N–S wind, and **f** wind speed

shifts in the location of the salinity fronts. Because of the sharp gradient in salinity in the frontal region, both surface and bottom salinity can change significantly with a small shift in the frontal location. The temporal evolution of salinity variations roughly follows river discharges. The high flows in the spring of 1993/1994, 1996, 1998, and 2003/2004 (Fig. 14) resulted in salinity dips (net negative salinity change due to negative values in the spatial maps) in the following seasons. The dry periods of 1995 and 1999–2002 elevated the salinity in the Bay by up to 8. The correlation improves when comparing the time variation with river discharge anomaly (with 31 data points or 62-day running average) shown as the red line (scale by 1/500, i.e., 1 unit corresponds to 500 m³/s) in Fig. 14. The correlation coefficient between the two curves shown is as high as 0.84

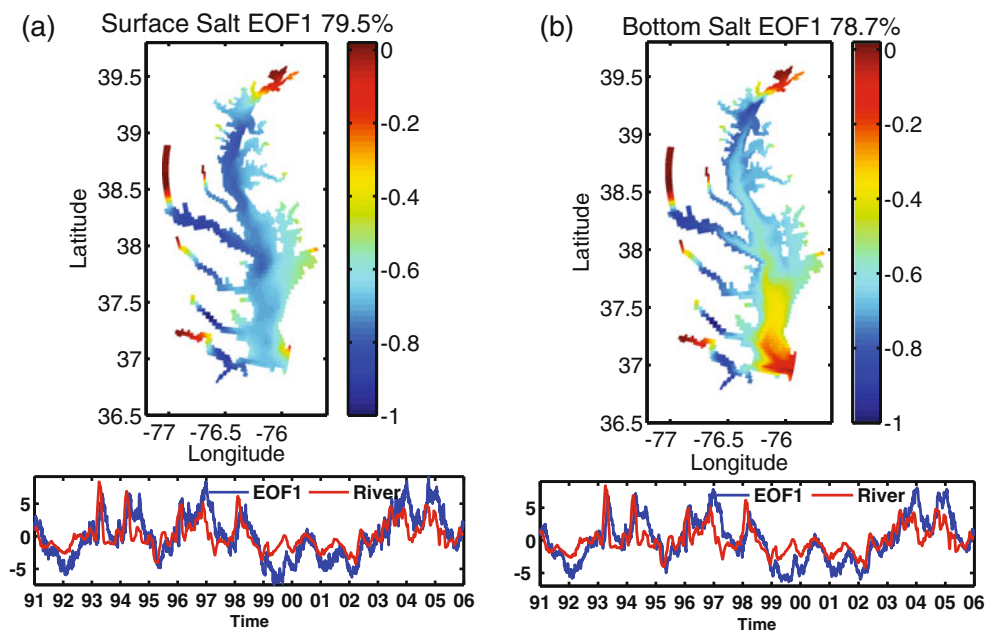
with a 32-day lead in river forcing. Seasonal averaging on both time series yields a correlation that reaches 0.92.

Austin's (2004) EOF analysis based on observed salinity at 21 main stem CBP stations showed that the first EOF of the depth integrated salinity explained 65% of the total variation and the temporal component was highly correlated (0.89) with the freshwater. The average of the spatial and temporal patterns from our Bay-wide surface and bottom analysis shows great similarities with Austin's (2004) results (refer to his Figs. 3c and 2c). Lee and Lwiza (2008) found that the bottom salinity was inversely related ($r=-0.71$) to the Susquehanna River discharge and the interannual and decadal variability in bottom salinity was also strongly affected by exchange with the ocean.

The remaining EOF modes only explain marginally more variance in surface and bottom salinity. For example, the second mode EOF only explains 5.3% of the variance in both surface and bottom salinity (Fig. 15). Locally, however, the salinity anomaly at some locations is greater than 5, which is comparable to the variation observed in the first mode. Both the surface and bottom temporal patterns show a much higher-frequency variation. The second mode of surface salinity displays a striking northeast–southwest dipole pattern. When salinity in the lower Bay increases, the salinity in the mid- to upper Bay decreases, and vice versa. Again, the bottom salinity change is considerably smaller than surface salinity, except in the James and York Rivers. And the northeast–southwest pattern is not as pronounced as in the surface.

The longitudinal wind component appears to have a role in driving this mode of salinity variation. In Fig. 15, the red lines are the N–S wind anomaly calculated using the NARR dataset after taking a 30-day running mean. When there is positive anomaly (i.e., stronger southerlies), the wind blows stronger against the typically prevailing southward flow of surface freshwater. The surface water is pushed northward by the wind and freshwater is relatively confined to the mid to upper Bay and this sets up the water surface against the head of the Bay. As a consequence, a more pronounced along-Bay pressure gradient drives a bottom layer outflow. The relaxation of strong northward wind reverses the process, leading to an along-Bay seiche (Wang 1979b; Wang and Elliott 1978). These salinity responses to contrasting N–S wind forcing conditions agree with the description of the wind-induced straining of the estuarine density field in Scully et al. (2005). The correlation between the second mode salinity variation in the surface and the bottom with N–S wind anomaly is moderate ($R=0.58$ and $R=0.53$, respectively), with a phase lag of 18 and 16 days. The downward spikes in the temporal patterns of surface and bottom salinity EOF2 in 1993, 1994, 1996, and 1998 coincide with the freshet events in those years.

Fig. 14 First EOF modes of **a** surface and **b** bottom salinity anomaly. The time series of the first EOF modes (*blue line*) showed strong correlation with river discharge anomaly with 60-day running mean (which is scaled by 1/500, i.e., 1 unit corresponds to 500 m³/s)



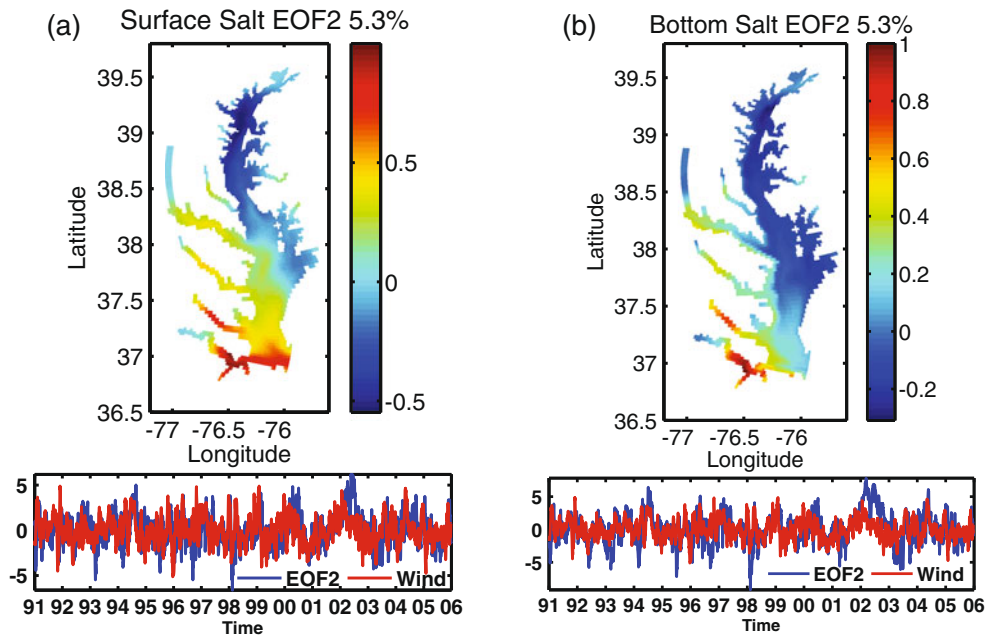
What we examined here is the effect of local winds on salinity. Hilton et al. (2008) illustrated that the offshore winds (far field) also affect salinity within the Bay through Ekman transport in/out of the Bay mouth.

Stratification

As mentioned above, the bottom to surface salinity difference is used as a proxy for water column salinity stratification. The first mode EOF explains nearly half of the variation in salinity stratification and has a magnitude of up to 10, shown as peaks during 2003 and 2004 (Fig. 16a).

Spatially, the stratification has little variation in the shallow areas along the shores where the water column tends to be well mixed. The area with largest variability resides in the lower Bay and over the deep channel in the main stem. The temporal pattern shows a low-frequency modulation of the high-frequency variation. After applying a 240-day moving average, the temporal pattern correlates positively ($R=0.93$) with the river discharge anomaly (Fig. 16a, red line), with the river forcing leading the vertical stratification response by 64 days (Fig. 17a). Therefore, the seasonal and interannual variability in salinity stratification in the Bay appears to be mainly driven by river discharge fluctuations.

Fig. 15 Second EOF modes of **a** surface and **b** bottom salinity anomaly. Superimposed on the time series of the second EOF mode is the 30-day running averaged N–S wind



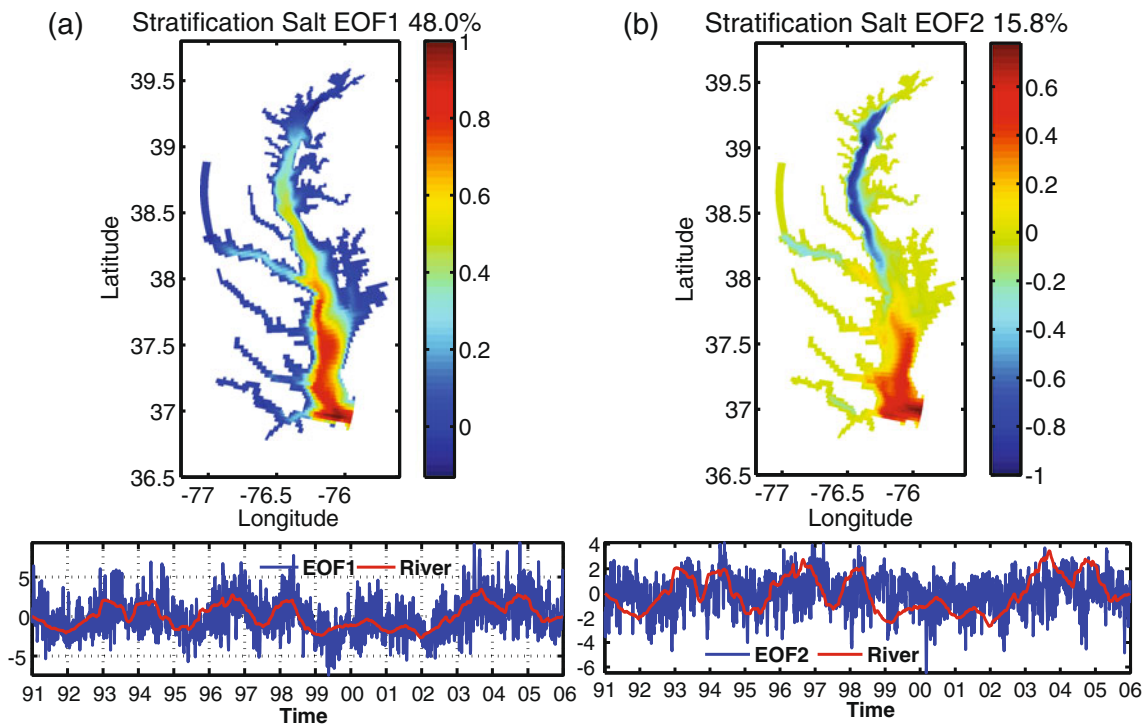


Fig. 16 **a** First and **b** second EOF modes of salinity stratification (represented by bottom surface salinity difference) and 240-day running averaged river discharge anomaly (scaled by $1/500 \text{ m}^3/\text{s}$)

Positive river discharge anomalies enhance stratification. After removing the low-frequency variability from the original pattern, the remaining time series does not show

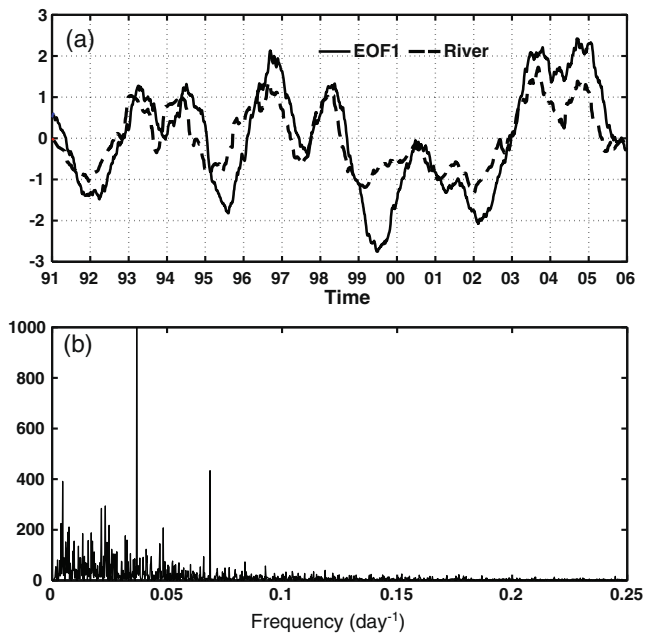


Fig. 17 **a** 240-day running mean of the first EOF mode of salinity stratification and river discharge anomaly (scaled by $1/1,000 \text{ m}^3/\text{s}$). **b** The raw power spectrum of first mode EOF of salinity stratification after removing the low-frequency variation shown in **a**

a clear connection with model forcing (not shown). However, the power spectrum of the residual temporal pattern reveals two dominant frequencies: one at 14.50 days and the other at 27.14 days (Fig. 17b). We speculate that this part of the stratification variability results from the residual signal of tidal mixing. The 14.50- and 27.14-day frequencies are close to the spring–neap cycle. Notably, the M_2 tide is the dominant tidal constituent in the Bay (Table 3) and the speed difference between M_2 and S_2 gives rise to a spring–neap cycle in tidal water level. The analysis is made on the 2-day averaged field so that, except for S_2 , the tidal effect is not completely filtered out. Here the difference between the period of the M_2 tide and the averaging process retains a fairly strong tidal signal at the frequency of the spring–neap cycle.

The first EOF mode of salinity stratification in Austin (2004) showed similar spatial pattern, with higher variations in the lower Bay. His spatial pattern was probably more uniform because salinity difference between 1 and 10 m was used as a proxy of vertical stratification, in contrast to the surface and bottom salinity difference used in this study. In addition, the low-frequency pattern in our temporal time series is also consistent with Austin’s (2004, Fig. 2d). However, broader high-frequency signal content is retained in the present study because we used 2-day averaged anomaly while Austin’s (2004) study was based on biweekly or monthly data.

The second EOF mode of bottom surface salinity difference explains an additional 16% of variance (Fig. 16b), which is significant and clearly separated relative to the first mode. The spatial variability also displays a distinct north–south dipole pattern in the main stem of the Bay, with the change in the lower Bay out of phase with the change over the deep channel in the mid- to upper Bay. The EOF2 time series and N–S wind anomaly show moderate correlation ($R=0.43$) with wind forcing leading by 2 days. Positive anomaly (stronger up-estuary winds) destratifies the water column and negative anomaly (strong down-estuary winds) enhances the vertical stratification by affecting the circulation pattern and inducing straining of the estuarine density field (Scully et al. 2005).

The temporal evolution of the second EOF mode does not seem to correlate with river forcing (Fig. 16b). Interestingly, after applying a 240-day moving average, the time series of the second EOF mode exhibits a very good correlation with the river discharge anomaly ($R=0.78$). In contrast to the direct response of whole bay stratification to variation in freshwater input revealed by the first mode, the second EOF mode indicates distinct responses to fluctuations in river discharge between the mid to upper Bay versus the lower Bay. This may reflect the difference between the two end members, with unstratified freshwater at one end and the stratified seawater at the other end. With strong river forcing, a larger area in the upper to mid-Bay could be dominated by freshwater input with little or no stratification. However, the enhanced two-layer circulation will result in higher stratification in the lower Bay. Apparently, the low-frequency changes in EOF2 illustrate such a secondary response to river discharge fluctuations. A similar dipole pattern, albeit weaker, can also be observed in the major tributaries.

Salinity Variability Along the Longitudinal Transect

An EOF analysis of the 2-day averaged salinity anomaly field on a longitudinal transect that roughly follows the deep channel in the upper to mid-Bay and extends south toward the Bay mouth (Fig. 1a) provides similar results to those obtained for the plane view of the salinity field. The first mode of EOF on the longitudinal–vertical transect dominates and explains 86% of the variance (Fig. 18a). At the uppermost reaches of the Bay and near the bottom of the Bay mouth, the salinity remains nearly constant from year to year, due to the large Susquehanna freshwater input and the high and relatively constant oceanic salinity conditions, respectively. The greatest salinity changes (up to 8) appear roughly 40 km down-Bay from the northern end of the transect. This is the region where the salinity front resides and corresponds to the confluence of sea water and the freshwater. The high variability in this area depicts

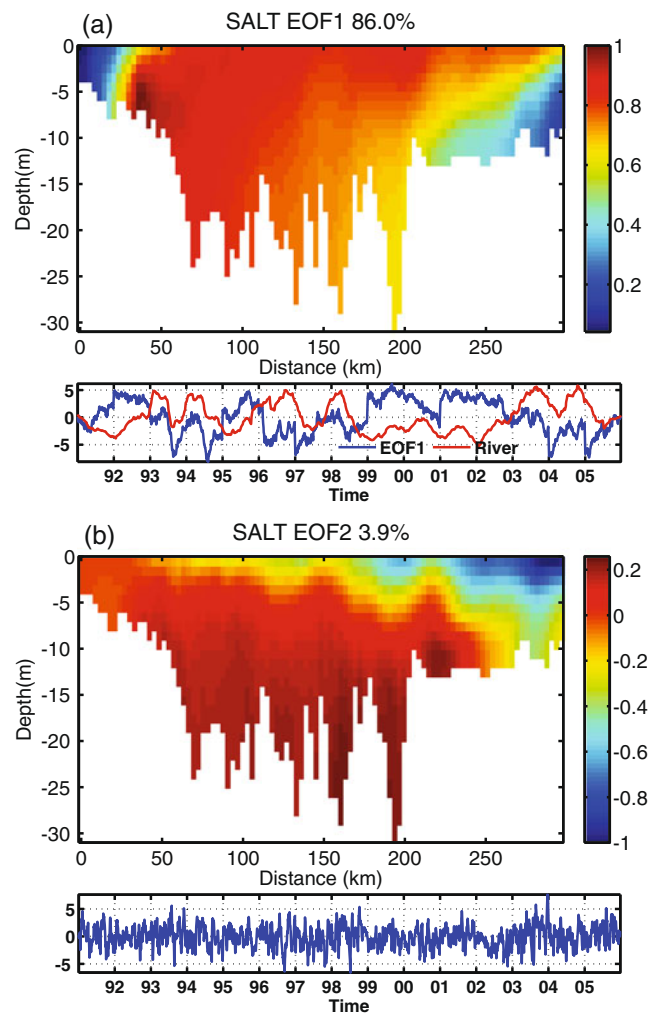


Fig. 18 a First and b second EOF modes for salinity anomaly along the longitudinal transect and the 180-day running averaged river discharge anomaly (scaled by $1/500 \text{ m}^3/\text{s}$) in a

the range and variation of the location of the salinity gradient in the estuary from fresh to salt water.

The temporal variation of longitudinal salinity distribution is similar to that noted in the surface and bottom salinity (Fig. 14) and is also greatly influenced by river discharge. For example, following the two spring freshet events in 1993 and 1994, the salinity in the high variability region dropped by about 7 in those two years and the prolonged dry periods of 1991–1992 and 1999–2002 resulted in the long periods of high salinity along the Bay relative to climatology. After applying a 120-day running mean, the correlation coefficients between the temporal evolution of EOF1 and river discharge anomaly reach -0.92 with a time lag of about 150 days. The coefficient is -0.98 when annual means are considered.

The second EOF mode (Fig. 18b) explains only about 4% of the variability but shows very interesting patterns.

The spatial variation of the salinity along the transect shows that the changes in the upper layer in the mid to lower Bay are out of phase from those in the deep channel. The time series of the second EOF mode indicates a prominent component of high-frequency variability. After applying a 240-day running mean, the temporal pattern is highly correlated with the N–S wind anomaly ($R=0.61$). The different salinity responses in the upper and lower Bay indicate the interaction between the wind-driven and density-induced circulation as discussed in the “Surface and Bottom Salinity” section. Winds combined with river discharge anomalies can explain about 57% of the seasonal EOF 2 temporal pattern. North–South wind alone explains 37% and adding river and E–W wind anomaly increases the explained variance by about 15% and 5%, respectively.

The same analysis was repeated on daily salinity anomaly along the transect (results not shown) to test the effect of the 2-day averaging on the analysis. The spatiotemporal patterns of the top EOF modes, as well as the correlation with both the river and wind forcing, are indistinguishable between the two analyses. Only slight changes in the explained variance and correlation coefficient were noticed. For example, the first two EOF modes from daily anomaly explained, respectively, 85.1% and 4.0% of the total variability and the correlation of the N–S wind anomaly and the EOF2 temporal time series changed from 0.61 to 0.59.

River Discharge Variability and Climate Patterns

River discharge in this region is affected by snowmelt, precipitation, and other factors such as soil moisture, etc, which in turn are affected by broader climate patterns. A close examination of the 15-year time series of total river discharge into the Bay and the major climate indices reveals that the River Flow Index (defined as the normalized monthly river discharge anomaly) closely follows the Pacific Decadal Oscillation (PDO) (Fig. 19, PDO data obtained from <http://jisao.washington.edu/pdo/>). The PDO index is defined as the leading principal component of the EOF of monthly sea surface temperature anomalies in the North Pacific Ocean (poleward of 20° N) (Mantua et al. 1997; Zhang et al. 1997). With the PDO leading by 8 months, the correlation coefficient between monthly PDO and the river flow index reaches 0.49 for the 15-year period (Fig. 19b). Further studies are needed to fully understand the teleconnection and the phase shift between the two. Prasad et al. (2010) showed that the total river discharge into the Bay was also significantly related to two other climatic indices: the North Atlantic Oscillation and ENSO. Nigam et al. (1999) argued that the persistence of drought patterns over continental USA is related to the PDO. These studies clearly demonstrate the influence of larger

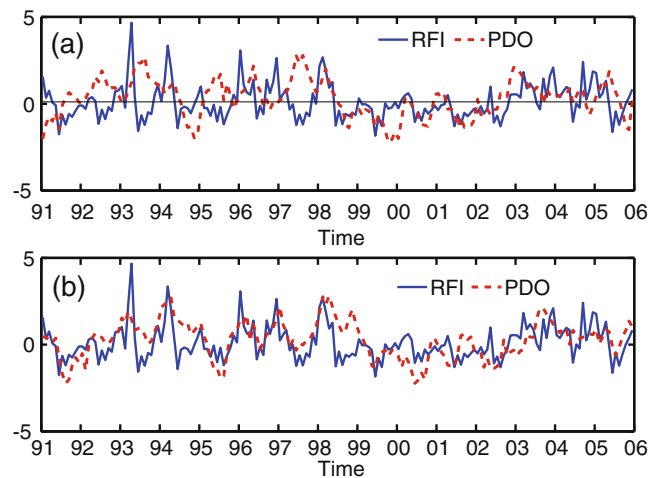


Fig. 19 **a** River Flow Index (RFI) and Pacific Decadal Oscillation (PDO) index in 1991–2005. **b** RFI in 1991–2005 with PDO leading 8 months (PDO shown is from May 1990 to April 2005)

climate variability patterns on the regional runoff, which consequently has profound impacts on the circulation and salt budget inside the Bay.

Summary and Conclusions

ChesROMS has been developed and validated through analysis of a 15-year retrospective simulation. The overall performance of the present modeling system provides confidence in its applicability as a forecast system despite the complexity of the actual physical system. The model is able to reproduce tidal propagation and temperature variation accurately. The model captures the essential salinity structure and its variability within the Bay. However, the skill of the model in capturing salinity variability is significantly less than that for temperature. This reduced skill for salinity simulation appears to be related to model resolution in both the horizontal and vertical directions and potentially to the choice of the turbulence mixing scheme.

Chesapeake Bay is, on average, a shallow system, but it has a narrow and deep channel along the Bay center line. The present model resolution (~2 km) tends to underestimate the depth of the deep channel, especially in the mid-Bay to upper Bay regions where the channel is particularly narrow. This loss of accuracy in representing the actual bathymetry effectively blocks the pathway of the bottom salinity intrusion, which contributes to the underestimation of salinity in bottom waters of the upper Bay and the overestimation of salinity in the mid-Bay. On the other hand, the accuracy of surface winds, tides, and non-tidal water elevation at the open ocean boundary needs to be

improved for better representation of the actual forcing. We should also keep in mind that the treatment of the C&D Canal in the present study is still highly experimental and idealized. The current treatment only provides an extra, though computationally inexpensive, degree of freedom to tune model results with the artificial inflow rate. More comprehensive modeling studies that treat the canal as an open ocean condition with forcing obtained from measured water level, temperature, and salinity at the Delaware Bay side of the canal are being conducted.

Based on data collected from 1991 to 2005, the river runoff and winds display a very strong seasonal cycle and large interannual variability in the Chesapeake Bay region. The seasonal and interannual variability in the forcing produces prominent seasonal and interannual variability in salinity structures in the Bay. The modeled Bay-wide salinity climatology (Fig. 13b) illustrates a dominant seasonal pattern in response to river discharge. A roughly 60-day (high flow period) to 80-day (low flow period) lag in the response time is seen, indicating that the residence time changes significantly with river discharge. Hagy et al. (2000) also found that the residence time of the Patuxent River estuary decreases with increasing river flow using a box model. From the EOF analysis (Figs. 14 and 16), we conclude that river forcing is the dominant factor contributing to seasonal and interannual variability of salinity in the Bay. This finding may be considered unremarkable. However, quantification of the relative dominance of the leading modes of salinity patterns and the similarities of the surface and the bottom salinities do offer new insights that are critical for the forecast exercise, especially in terms of potential extensions to ecological forecasts (Anderson et al. 2010; Constantin De Magny et al. 2010; Prasad et al. 2011).

It is interesting that, although the first EOF modes of both surface and bottom salinity show dominant low-frequency (seasonal scale) features (Fig. 14), the bottom surface salinity difference—a measure of stratification—displays a significant amount of high-frequency variability. River discharge variability can explain most of the seasonal and interannual changes in the surface and bottom salinity values. However, it cannot fully explain the short time scale changes in water column stratification. This clearly indicates that although river forcing dominates the overall salt content in the Bay, other forcing mechanisms, including winds and tides, can have a significant role as river forcing on salinity stratification structures. The Bay is typically stratified in late spring and summer because of high river discharge in spring and calm winds in summer. Strong winds in the fall and winter along with surface cooling tend to destratify and homogenize the water column. It is likely that the dominance of freshwater forcing by the river discharge itself provides a mechanism for trapping momentum in shallow mixed layers, the variability of which may

generate higher-frequency stratification changes due to processes such as shear-mixing. The present model results also indicate that residual tidal currents can have a significant role in determining the salinity structure (Fig. 17b). The salinity stratification variation showed a strong signal at 14.5 and 27.14 days based on the 2-day averaged salinity field. This agrees with Li and Zhong (2009), which showed that spring–neap modulation of tides can produce strong fortnightly and monthly signals in turbulent mixing and stratification.

The response of the Bay to wind forcing is complicated and dependent on wind direction, duration, and strength. Both long time scale and short time scale responses of the estuarine system are found to be related to wind. The conclusion that winds drive Bay circulation and influence the salinity structure at both short and long time scales also agrees with the findings by Wang and Elliott (1978), where sea level fluctuations of periods 20, 5, and 2.5 days were seen to be driven by continental coastal winds, local lateral winds (E–W winds), and local longitudinal winds (N–S winds). Goodrich and Blumberg (1991) also demonstrated that persistent longitudinal winds during low flow seasons can produce circulation with low-frequency features. Scully et al. (2005) demonstrated that the straining effect of along-estuary winds controls the effectiveness of wind and tidal mixing.

Based on the EOF analysis, the overall salt content and gradient in the Bay and the seasonal and interannual variation can be well predicted from river forcing. However, winds and tides can be equally important at shorter time scales in determining the actual salinity structures in the Bay.

The present model's configuration used climatology for temperature and salinity at the open ocean boundary. Therefore, the interannual to decadal variation in coastal ocean salinity associated with the Gulf Stream (Lee and Lwiza 2008) was not taken into account. As a result, the contribution from varying salinity in the adjacent ocean was absent from the model-based analysis presented here. In Hilton et al. (2008), the shelf salinity variation explained around 35% of their statistical model salinity residual. For future studies, we consider that providing a more accurate representation of bottom topography to allow more realistic deep salinity transport in the thalweg is probably the most important modification that can be made to the model to improve its simulation of salinity variability. Further improvements can likely be obtained by taking the open ocean boundary conditions from a regional model to capture the open ocean salinity variability influences on total salt flux into the Bay. Further investigation on the influences of the specification of the C&D Canal and improvement on the turbulent mixing closure and forcing accuracy are also needed to improve the salinity prediction.

Acknowledgments Funding for this study was provided by the National Oceanic and Atmospheric Administration's (NOAA) Center for Sponsored Coastal Ocean Research's Monitoring for Event Response for Harmful Algal Bloom (MERHAB) Program (NA05NOS4781222 and NA05NOS4781226 to PIs R. Hood and C. Brown, respectively) and the Center for Satellite Applications and Research. The authors thank Tom Gross for introducing ROMS to this project and helping with the initial model development and Frank Aikman and Edward Myers at NOAA/CSDL for generously supporting the completion of the model analyses and development of the manuscript. Murtugudde gratefully acknowledges the generous support of NOAA-CBFS grant and Divecha Center for Climate Change at

IISc, Bangalore. This paper represents UMCES contribution no. 4510 and MERHAB publication no. 150.

Appendix

In this appendix, the detailed statistics on model–observation comparisons at 38 main stem stations for 1998, 2001, and 2003, which represent normal, low, and high flow conditions, respectively, are listed in Table 5.

Table 5 Model performance evaluation for salinity in 1998, 2001, and 2003

Stations	Modeled		Observed		RMSE	MS	<i>R</i>	SS
	Mean	Std	Mean	Std				
Year 1998								
CB1.1	0.02	0.05	0.00	0.00	0.05	0.00	NaN	NaN
CB2.1	0.58	1.10	0.81	1.26	0.63	0.93	0.88	0.74
CB2.2	2.54	2.87	3.30	3.11	1.34	0.95	0.93	0.81
CB3.1	6.67	3.84	6.23	4.13	1.86	0.94	0.90	0.80
CB3.2	8.46	3.80	8.18	4.19	1.67	0.95	0.92	0.84
CB3.3C	11.37	3.19	11.95	4.27	2.47	0.89	0.83	0.66
CB3.3E	8.97	2.89	7.11	3.17	2.46	0.84	0.86	0.39
CB3.3W	9.04	2.90	7.35	3.34	2.37	0.86	0.87	0.50
CB4.1C	12.85	2.81	13.35	4.15	2.89	0.82	0.73	0.52
CB4.1W	9.66	2.75	8.16	3.19	1.89	0.90	0.94	0.66
CB4.2C	13.77	3.12	13.61	4.33	2.61	0.87	0.80	0.63
CB4.2E	12.12	2.48	9.33	3.00	3.04	0.77	0.92	−0.03
CB4.2W	9.85	2.81	8.48	3.03	1.66	0.92	0.95	0.70
CB4.3C	13.79	3.43	13.64	4.50	2.35	0.91	0.86	0.73
CB4.3E	13.10	2.48	12.27	3.66	2.52	0.82	0.76	0.52
CB4.3W	10.25	2.84	8.72	3.27	1.96	0.90	0.93	0.64
CB4.4	14.83	3.10	14.36	4.26	2.59	0.87	0.80	0.62
CB5.1	15.80	2.82	15.09	4.05	2.74	0.83	0.76	0.54
CB5.1W	13.26	3.24	11.83	3.61	2.09	0.91	0.91	0.67
CB5.2	16.31	3.07	15.09	4.12	2.42	0.89	0.87	0.65
CB5.3	17.56	3.41	15.72	4.24	2.54	0.89	0.92	0.64
CB5.4	19.33	3.16	17.04	3.88	2.72	0.86	0.94	0.52
CB5.4W	14.76	3.07	13.15	3.49	1.81	0.93	0.98	0.74
CB5.5	19.31	3.27	16.42	3.99	3.31	0.82	0.92	0.31
CB6.1	19.56	3.20	16.92	3.84	3.03	0.84	0.93	0.38
CB6.2	19.56	3.78	17.52	4.08	2.80	0.88	0.88	0.52
CB6.3	21.08	3.92	18.83	3.67	2.72	0.88	0.92	0.45
CB6.4	21.18	2.92	19.64	3.22	2.06	0.89	0.91	0.60
CB7.1	20.79	2.29	19.13	3.13	2.38	0.82	0.84	0.41
CB7.1N	19.38	2.14	16.65	2.67	3.03	0.72	0.87	−0.29
CB7.1S	21.53	3.27	19.10	3.88	2.98	0.84	0.90	0.41
CB7.2	23.96	3.25	21.97	3.56	2.69	0.85	0.86	0.42
CB7.2E	23.39	2.55	21.31	2.72	2.56	0.79	0.84	0.11
CB7.3	24.82	2.91	23.43	4.00	2.29	0.89	0.91	0.67

Table 5 (continued)

Stations	Modeled		Observed		RMSE	MS	R	SS
	Mean	Std	Mean	Std				
CB7.3E	24.74	2.46	23.33	2.82	1.96	0.87	0.88	0.52
CB7.4	27.35	3.12	26.89	3.21	1.47	0.94	0.90	0.78
CB7.4N	27.57	2.21	26.47	3.70	2.48	0.82	0.83	0.55
CB8.1	22.74	3.94	21.31	4.32	2.36	0.92	0.90	0.70
Year 2001								
CB1.1	0.00	0.01	0.00	0.00	0.01	0.00	NaN	NaN
CB2.1	0.66	0.71	1.02	1.19	0.72	0.86	0.90	0.63
CB2.2	3.15	2.01	4.57	3.11	2.80	0.71	0.63	0.19
CB3.1	9.72	2.55	8.86	3.54	2.40	0.84	0.78	0.55
CB3.2	11.32	2.73	11.27	3.59	2.18	0.87	0.79	0.62
CB3.3C	14.28	2.32	15.12	3.57	1.97	0.89	0.90	0.69
CB3.3E	12.67	2.42	11.75	2.72	2.01	0.84	0.76	0.45
CB3.3W	11.72	2.55	11.20	2.74	1.79	0.88	0.79	0.57
CB4.1C	16.23	1.53	16.83	3.08	2.11	0.78	0.82	0.53
CB4.1W	13.32	1.80	12.60	2.37	1.64	0.84	0.78	0.52
CB4.2C	17.14	1.91	16.99	3.05	1.79	0.86	0.84	0.66
CB4.2E	15.74	1.52	13.94	1.74	2.08	0.70	0.80	-0.44
CB4.2W	13.92	1.85	13.15	2.45	1.55	0.87	0.84	0.60
CB4.3C	17.27	2.16	17.24	3.12	1.71	0.89	0.85	0.70
CB4.3E	16.94	1.53	16.33	2.61	1.80	0.81	0.78	0.52
CB4.3W	14.48	1.89	13.46	2.43	1.78	0.83	0.80	0.46
CB4.4	18.39	1.73	18.13	3.07	1.95	0.82	0.82	0.60
CB5.1	18.95	1.43	18.85	2.88	2.05	0.75	0.74	0.49
CB5.1W	16.68	1.40	15.68	2.05	1.62	0.80	0.79	0.37
CB5.2	19.53	1.72	18.87	2.68	1.71	0.85	0.83	0.59
CB5.3	20.75	2.04	19.47	2.92	2.05	0.83	0.85	0.51
CB5.4	21.88	1.81	19.62	1.98	2.46	0.71	0.87	-0.55
CB5.4W	18.46	1.25	17.16	1.61	1.56	0.76	0.84	0.05
CB5.5	21.80	1.64	19.41	1.74	2.61	0.64	0.80	-1.27
CB6.1	22.06	1.81	20.21	1.98	2.28	0.71	0.76	-0.32
CB6.2	22.08	2.05	20.57	2.08	2.07	0.77	0.76	0.00
CB6.3	22.70	2.14	21.23	2.17	2.06	0.79	0.78	0.11
CB6.4	23.34	1.97	23.15	2.37	1.20	0.92	0.86	0.73
CB7.1	23.12	1.01	21.13	1.34	2.18	0.57	0.75	-1.64
CB7.1N	21.52	0.98	19.12	1.05	2.48	0.47	0.81	-4.58
CB7.1S	23.82	1.82	22.26	1.96	2.11	0.72	0.72	-0.16
CB7.2	25.56	1.76	24.29	2.59	2.02	0.80	0.81	0.40
CB7.2E	25.49	1.24	23.92	1.79	1.90	0.71	0.80	-0.14
CB7.3	26.78	2.16	26.19	2.70	1.54	0.90	0.85	0.67
CB7.3E	26.89	1.31	25.87	1.82	1.60	0.76	0.74	0.23
CB7.4	28.16	1.75	28.66	2.01	1.42	0.85	0.76	0.50
CB7.4N	29.21	1.12	29.96	2.28	1.95	0.67	0.62	0.26
CB8.1	24.17	2.23	24.53	2.15	1.34	0.90	0.83	0.62
Year 2003								
CB1.1	0.00	0.00	0.00	0.00	0.00	0.00	NaN	NaN
CB2.1	0.08	0.24	0.12	0.47	0.53	0.23	0.00	-0.27
CB2.2	1.06	1.38	2.17	2.90	2.62	0.62	0.58	0.18

Table 5 (continued)

Stations	Modeled		Observed		RMSE	MS	R	SS
	Mean	Std	Mean	Std				
CB3.1	5.26	2.94	6.51	4.14	3.12	0.79	0.72	0.43
CB3.2	7.13	2.81	8.18	4.03	2.41	0.87	0.86	0.65
CB3.3C	10.12	2.31	11.89	4.27	3.24	0.77	0.82	0.42
CB3.3E	8.79	1.92	8.06	2.02	1.52	0.85	0.77	0.43
CB3.3W	7.40	2.21	7.65	2.97	2.40	0.75	0.61	0.35
CB4.1C	12.20	1.83	13.77	4.06	3.29	0.71	0.77	0.34
CB4.1W	9.47	2.12	8.86	2.33	1.54	0.87	0.80	0.56
CB4.2C	13.26	2.13	13.64	4.03	2.65	0.80	0.81	0.57
CB4.2E	11.83	1.67	9.66	1.94	2.60	0.65	0.69	-0.80
CB4.2W	10.00	1.64	9.50	1.92	1.33	0.85	0.77	0.52
CB4.3C	13.33	2.40	13.91	4.02	2.42	0.85	0.85	0.64
CB4.3E	13.15	1.92	13.75	3.78	2.77	0.75	0.73	0.46
CB4.3W	10.62	1.68	9.69	1.80	1.48	0.83	0.78	0.32
CB4.4	14.46	1.95	14.75	3.95	2.75	0.77	0.77	0.51
CB5.1	15.17	1.77	15.50	3.88	2.98	0.70	0.68	0.41
CB5.1W	12.53	1.84	11.36	1.69	1.75	0.77	0.73	-0.08
CB5.2	15.66	2.25	15.47	3.70	2.31	0.84	0.81	0.61
CB5.3	16.77	2.70	16.13	3.90	2.34	0.87	0.83	0.64
CB5.4	17.80	2.59	16.81	3.58	2.20	0.87	0.84	0.62
CB5.4W	13.90	1.46	12.12	1.29	1.94	0.66	0.85	-1.26
CB5.5	18.00	2.66	16.16	3.29	2.79	0.80	0.77	0.28
CB6.1	18.27	2.67	15.84	2.85	2.89	0.78	0.84	-0.03
CB6.2	17.98	2.94	16.24	2.90	2.74	0.78	0.74	0.11
CB6.3	19.00	3.20	17.11	3.04	2.57	0.84	0.84	0.27
CB6.4	20.11	2.71	19.34	3.17	1.84	0.90	0.85	0.66
CB7.1	19.13	2.18	17.85	2.55	2.03	0.82	0.79	0.37
CB7.1N	16.99	1.55	15.69	2.00	1.86	0.75	0.75	0.14
CB7.1S	20.30	2.72	18.38	3.08	2.76	0.79	0.77	0.19
CB7.2	22.78	2.78	20.85	3.89	3.22	0.78	0.75	0.32
CB7.2E	22.73	2.19	20.52	2.42	2.83	0.69	0.71	-0.37
CB7.3	23.72	3.38	23.11	3.71	2.20	0.90	0.82	0.64
CB7.3E	24.37	2.24	22.93	2.52	2.19	0.80	0.77	0.25
CB7.4	27.33	2.97	26.91	3.55	2.29	0.87	0.77	0.57
CB7.4N	27.63	2.23	27.22	2.51	2.41	0.72	0.50	0.07
CB8.1	21.56	3.62	21.78	4.09	1.80	0.94	0.90	0.81

Measures listed are: modeled mean, modeled standard deviation (Std), observed mean, observed standard deviation, root mean square errors (RMSE), model skill (MS), correlation coefficient (*R*), and skill score (SS)

References

- Allen, J.I., P.J. Somerfield, and F.J. Gilbert. 2007. Quantifying uncertainty in high-resolution coupled hydrodynamic-ecosystem models. *Journal of Marine Systems* 64: 3–14.
- Anderson, C.R., et al. 2010. Predicting potentially toxigenic *Pseudo-nitzschia* blooms in the Chesapeake Bay. *Journal of Marine Systems* 83: 127–140.
- Austin, J.A. 2002. Estimating the mean ocean-bay exchange rate of the Chesapeake Bay. *Journal of Geophysical Research-Oceans* 107: 3192.
- Austin, J.A. 2004. Estimating effective longitudinal dispersion in the Chesapeake Bay. *Estuarine Coastal and Shelf Science* 60: 359–368.
- Calvo, G.W., M.W. Luckenbach, S.K. Allen Jr., and E.M. Burreson. 2001. A comparative field study of *Crassostrea ariakensis* (Fujita 1913) and *Crassostrea virginica* (Gmelin 1791) in relation to salinity in Virginia. *Journal of Shellfish Research* 20: 221–229.

- Chapman, D.C. 1985. Numerical treatment of cross-shelf open boundaries in a barotropic coastal ocean model. *Journal of Physical Oceanography* 15: 1060–1075.
- Constantin De Magny, G., et al. 2010. Predicting the distribution of *Vibrio* spp. in the Chesapeake Bay: A *Vibrio cholerae* case study. *EcoHealth* 6: 378–389.
- Dekshenieks, M.M., E.E. Hofmann, and E.N. Powell. 1993. Environmental effects on the growth and development of eastern oyster, *Crassostrea virginica* (Gmelin, 1791) larvae: A modeling study. *Journal of Shellfish Research* 12: 241–254.
- Dong, B.W., R.T. Sutton, S.P. Jewson, A. O'Neill, and J.M. Slingo. 2000. Predictable winter climate in the North Atlantic sector during the 1997–1999 ENSO cycle. *Geophysical Research Letters* 27: 985–988.
- Elliott, A.J., D.P. Wang, and D.W. Pritchard. 1978. The circulation near the head of Chesapeake Bay. *Journal of Marine Research* 36: 643–655.
- Flather, R.A. 1976. A tidal model of the northwest European continental shelf. *Mémoires Société Royale des Sciences de Liège* 6: 141–164.
- Foreman, M.G.G. 1977. *Manual for tidal heights analysis and prediction*, 97. Patricia Bay, Victoria: Institute of Ocean Science.
- Fulford, R.S., D.L. Breitburg, R.I.E. Newell, W.M. Kemp, and M. Luckenbach. 2007. Effects of oyster population restoration strategies on phytoplankton biomass in Chesapeake Bay: A flexible modeling approach. *Marine Ecology Progress Series* 336: 43–61.
- Gibson, J.R., and R.G. Najjar. 2000. The response of Chesapeake Bay salinity to climate-induced changes in streamflow. *Limnology and Oceanography* 45: 1764–1772.
- Goodrich, D.M., and A.F. Blumberg. 1991. The fortnightly mean circulation of Chesapeake Bay. *Estuarine Coastal and Shelf Science* 32: 451–462.
- Grötzner, A., M. Latif, and D. Dommengat. 2000. Atmospheric response to sea surface temperature anomalies during El Niño 1997/98 as simulated by ECHAM4. *Quarterly Journal of the Royal Meteorological Society* 126: 2175–2198.
- Guo, X.Y., and A. Valle-Levinson. 2007. Tidal effects on estuarine circulation and outflow plume in the Chesapeake Bay. *Continental Shelf Research* 27: 20–42.
- Hagy, J.D., L.P. Sanford, and W.R. Boynton. 2000. Estimation of net physical transport and hydraulic residence times for a coastal plain estuary using box models. *Estuaries* 23: 328–340.
- Haidvogel, D.B., et al. 2008. Ocean forecasting in terrain-following coordinates: Formulation and skill assessment of the Regional Ocean Modeling System. *Journal of Computational Physics* 227: 3595–3624.
- Haidvogel, D.B., H.G. Arango, K. Hedstrom, A. Beckmann, P. Malanotte-Rizzoli, and A.F. Shchepetkin. 2000. Model evaluation experiments in the North Atlantic Basin: Simulations in nonlinear terrain-following coordinates. *Dynamics of Atmospheres and Oceans* 32: 239–281.
- Hansen, D.V., and M.J. Rattray. 1965. Gravitational circulation in straits and estuaries. *Journal of Marine Research* 23: 104–122.
- Hicks, S. 1964. Tidal wave characteristics of Chesapeake Bay. *Chesapeake Science* 5: 103–113.
- Hilton, T.W., R.G. Najjar, L. Zhong, and M. Li. 2008. Is there a signal of sea-level rise in Chesapeake Bay salinity? *Journal of Geophysical Research* 113: C09002. doi:10.1029/2007JC004247.
- Johnson, B.H., R.E. Heath, B.B. Hsieh, K.W. Kim, and H.L. Butler. 1991. *Development and verification of a three-dimensional numerical hydrodynamic, salinity, and temperature model of Chesapeake Bay*. Vicksburg: US Army Corps of Engineers, Waterways Experiment Stations. 193.
- King, R.S., A.H. Hines, F.D. Craige, and S. Grap. 2005. Regional, watershed and local correlates of blue crab and bivalve abundances in subestuaries of Chesapeake Bay, USA. *Journal of Experimental Marine Biology and Ecology* 319: 101–116.
- Kranenburg, C. 1986. A time scale for long-term salt intrusion in well-mixed estuaries. *Journal of Physical Oceanography* 16: 1329–1331.
- Large, W.G., J.C. McWilliams, and S.C. Doney. 1994. Oceanic vertical mixing: A review and a model with a nonlocal boundary layer parameterization. *Reviews of Geophysics* 32: 363–403.
- Lee, Y.J., and K.M.M. Lwiza. 2008. Factors driving bottom salinity variability in the Chesapeake Bay. *Continental Shelf Research* 28: 1352–1362.
- Lerczak, J.A., W.R. Geyer, and D.K. Ralston. 2009. The temporal response of the length of a partially stratified estuary to changes in river flow and tidal amplitude. *Journal of Physical Oceanography* 39: 915–933.
- Li, M., and L. Zhong. 2009. Flood–ebb and spring–neap variations of mixing, stratification and circulation in Chesapeake Bay. *Continental Shelf Research* 29: 4–14.
- Li, M., L.J. Zhong, and W.C. Boicourt. 2005. Simulations of Chesapeake Bay estuary: Sensitivity to turbulence mixing parameterizations and comparison with observations. *Journal of Geophysical Research-Oceans* 110: 22.
- Maccready, P. 1999. Estuarine adjustment to changes in river flow and tidal mixing. *Journal of Physical Oceanography* 29: 708–726.
- Maccready, P. 2007. Estuarine adjustment. *Journal of Physical Oceanography* 37: 2133–2145.
- Mantua, N.J., S.R. Hare, Y. Zhang, J.M. Wallace, and R.C. Francis. 1997. A Pacific interdecadal climate oscillation with impacts on salmon production. *Bulletin of the American Meteorological Society* 78: 1069–1079.
- Mellor, G., and T. Yamada. 1982. Development of a turbulence closure model for geophysical fluid problems. *Reviews of Geophysics* 20: 851–875.
- Mukai, A.Y., J.J. Westerink, R.A. Luettich, and D. Mark. 2002. *Eastcoast 2001: A tidal constituent database for the western North Atlantic, Gulf of Mexico and Caribbean Sea*, 201. Vicksburg: US Army Corps of Engineers.
- Murphy, A.H. 1988. Skill scores based on the mean-square error and their relationships to the correlation-coefficient. *Monthly Weather Review* 116: 2417–2425.
- Najarian, T.O., D.R.F. Harleman, and M.L. Thatcher. 1980. C & D Canal effect on salinity of Delaware estuary. *Journal of the Waterway Port Coastal and Ocean Division* 106: 1–17.
- Nigam, S., M. Barlow, and E.H. Berbery. 1999. Analysis links Pacific decadal variability to drought and streamflow in United States. *EOS, Transactions American Geophysical Union* 80: 621.
- Oke, P.R., et al. 2002. A modeling study of the three-dimensional continental shelf circulation off Oregon. Part I: Model–data comparisons. *Journal of Physical Oceanography* 32: 1360–1382.
- Orth, R., and K. Moore. 1984. Distribution and abundance of submerged aquatic vegetation in Chesapeake Bay: A historical perspective. *Estuaries and Coasts* 7: 531–540.
- Prasad, M., W. Long, X. Zhang, R. Wood, and R. Murtugudde. 2011. Predicting dissolved oxygen in the Chesapeake Bay: Applications and implications. *Aquatic Sciences—Research Across Boundaries*: 1–15. doi:10.1007/s00027-011-0191-x.
- Prasad, M., M. Sapiano, C. Anderson, W. Long, and R. Murtugudde. 2010. Long-term variability of nutrients and chlorophyll in the Chesapeake Bay: A retrospective analysis, 1985–2008. *Estuaries and Coasts* 33: 1128–1143.
- Pritchard, D. 1960. Salt balance and exchange rate for Chincoteague Bay. *Chesapeake Science* 1: 48–57.
- Pritchard, D.W. 1952. Salinity distribution and circulation in the Chesapeake Bay estuarine system. *Journal of Marine Research* 11: 106–123.
- Pritchard, D.W., and G.B. Gardner. 1974. *Hydrography of the Chesapeake and Delaware Canal*, 77. Baltimore: Chesapeake Bay Institute.

- Ralston, D.K., W.R. Geyer, and J.A. Lerczak. 2010. Structure, variability, and salt flux in a strongly forced salt wedge estuary. *Journal of Geophysical Research-Oceans* 115: C06005.
- Sandoz, M., and R. Rogers. 1944. The effect of environmental factors on hatching, moulting, and survival of zoea larvae of the blue crab *Callinectes sapidus* Rathbun. *Ecology* 25: 216–228.
- Schubel, J.R., and D.W. Pritchard. 1986. Responses of upper Chesapeake Bay to variations in discharge of the Susquehanna River. *Estuaries* 9: 236–249.
- Scully, M., C. Friedrichs, and J. Brubaker. 2005. Control of estuarine stratification and mixing by wind-induced straining of the estuarine density field. *Estuaries and Coasts* 28: 321–326.
- Seitz, R.C. 1971. Drainage area statistics for the Chesapeake Bay freshwater drainage basin. Baltimore: The Chesapeake Bay Institute, p. 21.
- Shchepetkin, A.F., and J.C. McWilliams. 2005. The regional oceanic modeling system (ROMS): A split-explicit, free-surface, topography-following-coordinate oceanic model. *Ocean Modelling* 9: 347–404.
- Shen, J., and H.V. Wang. 2007. Determining the age of water and long-term transport timescale of the Chesapeake Bay. *Estuarine Coastal and Shelf Science* 74: 585–598.
- Song, Y.H., and D. Haidvogel. 1994. A semi-implicit ocean circulation model using a generalized topography-following coordinate system. *Journal of Computational Physics* 115: 228–244.
- Stickney, A.P. 1964. Salinity, temperature, and food requirements of soft-shell clam larvae in laboratory culture. *Ecology* 45: 283–291.
- Taylor, K.E. 2001. Summarizing multiple aspects of model performance in a single diagram. *Journal of Geophysical Research* 106: 7183–7192.
- Thatcher, M., and T. Najarian. 1983. Transient hydrodynamic and salinity simulations in the Chesapeake Bay network. *Estuaries and Coasts* 6: 356–363.
- Wang, D.-P. 1979a. Subtidal sea level variations in the Chesapeake Bay and relations to atmospheric forcing. *Journal of Physical Oceanography* 9: 413–421.
- Wang, D.-P. 1979b. Wind-driven circulation in the Chesapeake Bay, winter, 1975. *Journal of Physical Oceanography* 9: 564–572.
- Wang, D., and A. Elliott. 1978. Non-tidal variability in the Chesapeake Bay and Potomac River: Evidence for non-local forcing. *Journal of Physical Oceanography* 8: 225–232.
- Wang, H.V., and B.H. Johnson. 2000. Validation and application of the second generation three dimensional hydrodynamic model of Chesapeake Bay. *Water Quality and Ecosystems Modeling* 1: 51–90.
- Ward, N.D., J.A. Gebert, and J.R. Weggel. 2009. Hydraulic study of the Chesapeake and Delaware Canal. *Journal of Waterway, Port, Coastal, and Ocean Engineering* 134: 24–30.
- Warner, J.C., W.R. Geyer, and J.A. Lerczak. 2005a. Numerical modeling of an estuary: A comprehensive skill assessment. *Journal of Geophysical Research-Oceans* 110: 13.
- Warner, J.C., C.R. Sherwood, H.G. Arango, and R.P. Signell. 2005b. Performance of four turbulence closure models implemented using a generic length scale method. *Ocean Modelling* 8: 81–113.
- Wilmott, C.J. 1981. On the validation of models. *Physical Geography* 2: 184–194.
- Wong, K.C. 1987. Subtidal volume exchange through the Chesapeake and Delaware Canal. *Journal of Geophysical Research-Oceans* 92: 10870–10874.
- Wong, K.C. 1990. The current and sea-level variability in the Chesapeake and Delaware Canal. *Journal of Geophysical Research-Oceans* 95: 18343–18352.
- Wong, K.C. 1991. The response of the Delaware estuary to the combined forcing from Chesapeake Bay and the ocean. *Journal of Geophysical Research-Oceans* 96: 8797–8809.
- Wong, K.C. 2002. On the spatial structure of currents across the Chesapeake and Delaware Canal. *Estuaries* 25: 519–527.
- Wong, K.C., and R.W. Garvine. 1984. Observations of wind-induced, subtidal variability in the Delaware Estuary. *Journal of Geophysical Research-Oceans* 89: 589–597.
- Xu, J.T., S.Y. Chao, R.R. Hood, H.V. Wang, and W.C. Boicourt. 2002. Assimilating high-resolution salinity data into a model of a partially mixed estuary. *Journal of Geophysical Research-Oceans* 107: 15.
- Zhang, Y., J.M. Wallace, and D.S. Battisti. 1997. ENSO-like interdecadal variability: 1900–93. *Journal of Climate* 10: 1004–1020.
- Zhong, L.J., and M. Li. 2006. Tidal energy fluxes and dissipation in the Chesapeake Bay. *Continental Shelf Research* 26: 752–770.